OUKA
The University of Osaka
Institutional Knowledge Archive

Title	Deletion of Trps1 regulatory elements recapitulates postnatal hip joint abnormalities and growth retardation of Trichorhinophalangeal syndrome in mice
Author(s)	Saeki, Naoya; Inui-Yamamoto, Chizuko; Ikeda, Yuki et al.
Citation	Human Molecular Genetics. 2024, 33(18), p. 1618-1629
Version Type	AM
URL	https://hdl.handle.net/11094/97151
rights	
Note	

The University of Osaka Institutional Knowledge Archive : OUKA

https://ir.library.osaka-u.ac.jp/

The University of Osaka

OXFORD UNIVERSITY PRESS | Human Molecular Genetics

Deletion of Trps1 regulatory elements recapitulates postnatal hip joint abnormalities and growth retardation of Trichorhinophalangeal syndrome in mice

Journal:	*Human Molecular Genetics*
Manuscript ID	HMG-2024-CE-00133.R1
Manuscript Type:	Original Article
Date Submitted by the Author:	n/a
Complete List of Authors:	Saeki, Naoya; Osaka University, Graduate School of Dentistry, Tissue and Dev Biol Inui-Yamamoto, Chizuko; Osaka University, Graduate School of Dentistry, Tissue and Dev Biol Ikeda, Yuki; Osaka University, Graduate School of Dentistry, Tissue and Dev Biol Kanai, Rinna; Osaka University, Graduate School of Dentistry, Tissue and Dev Biol Hata, Kenji; Osaka University, Graduate School of Dentistry, Department of Molecular and Cellular Biochemistry Itoh, Shousaku; Osaka University, Graduate School of Dentistry, Department of Fixed Prosthodontics and Orofacial Function Inubushi, Toshihiro; Osaka University, Graduate School of Dentistry, Department of Orthodontics and Dentofacial Orthopedics Akiyama, Shigehisa; Osaka University, Graduate School of Dentistry, Department of Special Needs Dentistry Ohba, Shinsuke; Osaka University, Graduate School of Dentistry, Tissue and Dev Biol Abe, Makoto; Osaka University, Graduate School of Dentistry, Tissue and Dev Biol
Key Words:	TRPS1, skeletal dysplasia, enhancer knockout, hip joint

SCHOLARONE™
Manuscripts

Deletion of Trps1 regulatory elements recapitulates postnatal hip joint abnormalities and growth retardation of Trichorhinophalangeal syndrome in mice

Naoya Saeki[1,2], Chizuko Inui-Yamamoto[1], Yuki Ikeda[1] , Rinna Kanai[1,3], Kenji Hata[4], Shousaku Itoh[5], Toshihiro Inubushi[6], Shigehisa Akiyama[2], Shinsuke Ohba[1,*], Makoto Abe[1,*]

[1]Department of Tissue and Developmental Biology, Osaka University Graduate School of Dentistry, Yamada-oka 1-8, Suita, Osaka 565-0871, Japan

[2]Department of Special Needs Dentistry, Osaka University Graduate School of Dentistry, Yamada-oka 1-8, Suita, Osaka 565-0871, Japan

[3]Department of Fixed Prosthodontics and Orofacial Function, Osaka University Graduate School of Dentistry, Yamada-oka 1-8, Suita, Osaka 565-0871, Japan

[4]Department of Molecular and Cellular Biochemistry, Osaka University Graduate School of Dentistry, Yamada-oka 1-8, Suita, Osaka 565-0871, Japan

[5]Department of Restorative Dentistry and Endodontology, Osaka University Graduate School of Dentistry, Yamada-oka 1-8, Suita, Osaka 565-0871, Japan

[6]Department of Orthodontics and Dentofacial Orthopedics, Osaka University

For Peer Review

Graduate School of Dentistry, Yamada-oka 1-8, Suita, Osaka 565-0871, Japan

* Corresponding author: Makoto Abe, Department of Tissue and Developmental Biology, Osaka University Graduate School of Dentistry, 1-8 Yamada-oka, Suita, Osaka 565-0871, Japan, Tel: +81-6-6879-2874, FAX: +81-6-6879-2875, Email: makoto.abe.dent@osaka-u.ac.jp

* Corresponding author: Shinsuke Ohba, Department of Tissue and Developmental Biology, Osaka University Graduate School of Dentistry, 1-8 Yamada-oka, Suita, Osaka 565-0871, Japan, Tel: +81-6-6879-2871, FAX: +81-6-6879-2875, Email: ohba.shinsuke.dent@osaka-u.ac.jp

For Peer Review

Abstract

Trichorhinophalangeal syndrome (TRPS) is a genetic disorder caused by point mutations or deletions in the gene-encoding transcription factor TRPS1. TRPS patients display a range of skeletal dysplasias, including reduced jaw size, short stature, and a cone-shaped digit epiphysis. Certain TRPS patients experience early onset coxarthrosis that leads to a devastating drop in their daily activities. The etiologies of congenital skeletal abnormalities of TRPS were revealed through the analysis of *Trps1* mutant mouse strains. However, early postnatal lethality in *Trps1* knockout mice has hampered the study of postnatal TRPS pathology. Here, through epigenomic analysis we identified two previously uncharacterized candidate gene regulatory regions in the first intron of *Trps1*. We deleted these regions, either individually or simultaneously, and examined their effects on skeletal morphogenesis. Animals that were deleted individually for either region displayed only modest phenotypes. In contrast, the *Trps1*$^{\Delta int/\Delta int}$ mouse strain with simultaneous deletion of both genomic regions exhibit postnatal growth retardation. This strain displayed delayed secondary ossification center formation in the long bones and misshaped hip joint development that resulted in acetabular dysplasia. Reducing one allele of the *Trps1* gene in *Trps1*$^{\Delta int}$ mice resulted in medial patellar dislocation that has been observed in some patients with TRPS. Our novel *Trps1* hypomorphic strain

For Peer Review

recapitulates many postnatal pathologies observed in human TRPS patients, thus positioning this strain as a useful animal model to study postnatal TRPS pathogenesis. Our observations also suggest that *Trps1* gene expression is regulated through several regulatory elements, thus guaranteeing robust expression maintenance in skeletal cells.

For Peer Review

Introduction

Trichorhinophalangeal syndrome (TRPS) is an autosomal-dominant genetic disorder caused by mutations or deletions in the transcription factor TRPS1 [1]. The occurrence rate of TRPS is extremely low and is estimated to be 1 in 50,000 live births [2]. Patients with TRPS display several congenital skeletal pathologies, including micrognathia, a cone-shaped epiphysis of the phalangeal bone, short stature, and hip joint dysplasia (OMIM #150230, #190350, #190351). Growth failure becomes pronounced as patients grow, and many patients suffer from early onset coxarthritis [3]. The role of TRPS1 during embryonic long bone development has been thoroughly investigated using murine models of TRPS [4-8]. The lack of *Trps1* in mice results in reduced chondrocyte proliferation and delayed hypertrophic differentiation of long bone epiphyseal and temporomandibular joint growth plates [5; 8]. These changes involve altered Wnt5a-, Pthlh-, Hedgehog-, and Stat3-mediated signaling due to the absence of *Trps1* [8-12]. In addition, altered growth plate characteristics indirectly lead to the uncoupling of growth plate maturation rate and perichondrial ossification in *Trps1* mutant mice, ultimately resulting in accelerated bone collar formation [6]. These observations underscore the crucial role of Trps1 during endochondral ossification of long bone.

Despite accumulating knowledge regarding TRPS1 during embryonic long bone

For Peer Review

development, the etiologies of postnatal skeletal pathologies of TRPS remain elusive [2]. Greater than 50% of patients with TRPS experience developmental dysplasia of the hip [2; 3; 13]. The femoral heads of young patients with TRPS display Perthes disease-like symptoms, although the damaged joints do not recover [14-18]. This clinical evidence indicates the crucial role(s) played by TRPS1 in the context of joint development and postnatal maintenance at various anatomical sites; however, few studies have described the exact roles played by Trps1 in hip joint development.

The hind limbs of tetrapods are derived from the pelvic fins of ancestral fishes [19]. Although the pelvic fins in fish are considered to play minor roles in swimming, they have clearly shifted to robust weight-bearing limbs in tetrapods [20]. The pelvic girdle connects the axial and hindlimb skeletons. Unlike the long bones, os coxae (hip bones) form through the gradual fusion of three initially separated bones, including the ilium, ischium, and pubis. Each bone piece is formed through endochondral ossification that is initiated by the condensation of mesenchymal cells originating from the mesodermal cells of the somatopleure [21]. The cartilage primordium of the ilium, ischium, and pubis fuses and establishes a complex triradiate zone at the site of the future acetabulum, where the femoral heads articulate. In humans, primary ossification centers are sequentially formed, first in the ilium primordium and then in the ischium and pubis

For Peer Review

[22]. Secondary ossification occurs at multiple locations in the pelvis that include the iliac crest, the pubic symphysis, and the ischial tuberosity [23]. The triradiate zone of the acetabulum remains un-ossified until mid-puberty and functions as a cartilaginous growth plate that allows the acetabulum to expand to accommodate the enlarging femoral head [24].

As the pelvis is one of the weight-bearing joints in all terrestrial animals, precise morphogenesis of the hip joint structure is crucial for locomotion. Indeed, the hip joint morphology appears quite delicate, and both under- and over-coverage of the acetabulum on the femur raises clinical issues such as acetabular dysplasia or femoroacetabular impingement (FAI) [25-27]. Severe under-coverage can cause hip instability, subluxation, or dislocation [28; 29]. Increased stress due to under-coverage is one of the causes of acetabular labral hypertrophy and tears that, in some cases, force joint surgery to prevent the onset of coxarthritis [30].

In this report, we describe developmental dysplasia of the hip during the embryonic stages in newly developed *Trps1* hypomorphic mouse strains. *Trps1* hypomorphic mice survived postnatally but displayed under-coverage of the femoral head in the acetabulum. Further reduction in *Trps1* gene dosage resulted in a reduced survival rate; however, surviving adult mice exhibited major skeletal abnormalities observed in human

For Peer Review

TRPS patients. These observations reinforce the crucial roles played by Trps1 in normal hip joint morphogenesis and partially explain the etiology of coxarthrosis observed in certain patients with TRPS.

For Peer Review

Results

1. Identification of putative enhancers in the first intron of the murine *Trps1* gene

Our previous study indicated that several *Trps1* regulatory sequence for its tissue-specific expression locates at the proximal promoter region of the *Trps1* gene [31]. As regulations of the *Trps1* gene transcription in several tissues were unclear from the previous study (e.g., growth plate chondrocytes and kidney ureteric bud), we aimed to identify other *Trps1* enhancers by uncovering the chromatin profiles at the *Trps1* gene locus in murine costal chondrocytes. Chondrocytes were used in this study, as *Trps1*$^{-/-}$ mice exhibit severe cartilage defects during the late embryonic stages [4; 6; 8; 10], and short stature is a prominent feature of postnatal human TRPS pathologies [2]. Chromatin accessibility (ATAC-seq) and histone modifications for active enhancer signatures (ChIP-seq for H3K27ac and H3K4me2) were assessed. Comparison of ATAC-seq and ChIP-seq peaks revealed that several open chromatin regions were accompanied with the active enhancer signatures (Fig. 1A). Among them, we found two prominent regions in the first intron of the *Trps1* gene body, each of which were approximately 3 kb (Enh2; Chr15:50885838-50889066) to 5 kb (Enh3; Chr15:50868499-50872947) in length (Fig. 1A). The identified mouse genomic sequence showed almost 75% homologies to human

For Peer Review

TRPS1 genomic sequences (Enh2, human Chr8:115664810-115668001; Enh3, human Chr8:115646975-115650605). Multispecies sequence alignment of the *Trps1* gene using the Evolutionary Conserved Regions (ECR) program Dcode.org (http://www.dcode.org) revealed that several intronic regions including Enh2 and Enh3, as well as the TSS proximal promoter region, were conserved between mice, humans, opossums, and chickens, while all exons displayed the highest conservation (Fig. 1B). Although frogs exhibited some alignment with other higher vertebrates within the fourth intron, similarities within the first intron were limited.

The Enh2 and Enh3 elements were cloned and inserted into a luciferase vector containing the minimum promoter. We performed luciferase assays using the vectors in ATDC5 chondrocytic cells to ask whether the two elements could induce transcriptional activation either individually or simultaneously (Fig. 1C). Enh2 augmented transcriptional activity, whereas Enh3 fragment did not (Fig. 1C). Furthermore, tandem constructs carrying both Enh2 and Enh3 induced less activities than those carrying Enh2 alone (Fig. 1C). To identify the responsible domain for transcriptional activation in Enh2, we analyzed luciferase activities using Enh2 deletion mutant constructs (each fragment of almost 1 kb in length). This assay revealed that two thirds in the 5' side of the Enh2 contains responsible elements for its activity (Fig. 1D).

For Peer Review

2. Individual deletion of Enh1, Enh2, and Enh3 causes mildly abnormal acetabular rim morphology when combined with heterozygous deletion of the *Trps1* gene

To investigate the potential *in vivo* roles of Enh2 and Enh3, we generated *Trps1*$^{\Delta Enh2/\Delta Enh2}$ and *Trps1*$^{\Delta Enh3/\Delta Enh3}$ mice, which lack Enh2 and Enh3 (Suppl. Fig. 1) using CRISPR/Cas9 genome editing. In addition to *Trps1*$^{\Delta Enh2/\Delta Enh2}$ and *Trps1*$^{\Delta Enh3/\Delta Enh3}$ mice, we also generated a mouse strain which lacks the majority of the previously identified proximal promoter sequences of *Trps1* gene (Enh1) while retaining the potential basal promoter sequence (*Trps1*$^{\Delta Enh1/\Delta Enh1}$; Suppl. Fig. 1) [31].

Trps1$^{\Delta Enh1/\Delta Enh1}$ mice were viable and gained body weight, and this did not differ from control (WT and *Trps1*$^{\Delta Enh1/+}$) mice (Suppl. Fig. 2A). *Trps1*$^{\Delta Enh2/\Delta Enh2}$ (Suppl. Fig. 2B) and *Trps1*$^{\Delta Enh3/\Delta Enh3}$ (Suppl. Fig. 2C) mice were also viable and gained body weight compared to their control mice. The genotype distribution at the weaning time were as predicted in all three strains, thus indicating that the Enh1 (Suppl. Fig. 2D), Enh2 (Suppl. Fig. 2E), and Enh3 (Suppl. Fig. 2F) sequence deletion did not affect the survival rate during this developmental period. As *Trps1* conventional knockout mice display numerous skeletal abnormalities at the embryonic stage, we analyzed *Trps1*$^{\Delta Enh1/\Delta Enh1}$, *Trps1*$^{\Delta Enh2/\Delta Enh2}$, and *Trps1*$^{\Delta Enh3/\Delta Enh3}$ neonates (PNd0; Suppl. Figs. 2G-2R). The

For Peer Review

morphology and sizes of the craniofacial (Suppl. Figs. 2G, 2J, 2M, and 2P), the forelimb skeletons (Suppl. Figs. 2H, 2K, 2N, and 2Q), and hindlimb (Suppl. Figs 2I, 2L, 2O, and 2R) appeared normal in *Trps1*$^{\Delta Enh1/\Delta Enh1}$ (Suppl. Figs. 2J-2L), *Trps1*$^{\Delta Enh2/\Delta Enh2}$ (Suppl. Figs. 2M-2O), and *Trps1*$^{\Delta Enh3/\Delta Enh3}$ (Suppl. Figs. 2P-2R) mice compared to the WT control mice (Suppl. Figs. 2G-2I).

The skeletal morphology of *Trps1*$^{\Delta Enh1/\Delta Enh1}$ (Suppl. Figs. 3C, 3K, and data not shown), *Trps1*$^{\Delta Enh2/\Delta Enh2}$ (Suppl. Figs. 3E, 3M, and data not shown), and *Trps1*$^{\Delta Enh3/\Delta Enh3}$ (Suppl. Figs. 3G, 3O, and data not shown) at the postnatal mature stage was overtly normal in 3D-CT images compared to the wild-type (Suppl. Figs. 3A, 3I, and data not shown) or *Trps1*$^{+/-}$ mice (Suppl. Figs. 3B, 3J, and data not shown). However, simultaneous deletion of Enh1 and another allele of *Trps1* gene (*Trps1*$^{\Delta Enh1/-}$), which was assumed to result in reduced baseline *Trps1* expression compared to homozygous deletion of Enh1 (*Trps1*$^{\Delta Enh1/\Delta Enh1}$), resulted in deeper invagination of the psoas valley of the hip joint than the other control mice (Suppl. Fig. 3D). The knee joints of *Trps1*$^{\Delta Enh1/-}$ mice appeared normal in both 3D-CT images and histological sections (Suppl. Figs. 3L and data not shown). *Trps1*$^{\Delta Enh2/-}$ (Suppl. Fig. 3F) and *Trps1*$^{\Delta Enh3/-}$ (Suppl. Fig. 3H) mice, which one allele of the *Trps1* gene was deleted, also showed modestly deepened psoas valley, which resulted in a small under-coverage of the femoral head by the acetabulum. Knee joints

For Peer Review

of *Trps1*$^{\Delta Enh2/-}$ (Suppl. Figs. 3N and data not shown) and *Trps1*$^{\Delta Enh2/-}$ (Suppl. Fig. 3P and data not shown) mice appeared normal in both 3D-CT images and histological sections. Thus, individual deletions of Enh1, Enh2, or Enh3 only result in modest skeletal phenotypes in mice.

3. *Trps1*$^{-/-}$ mouse embryos show defects in pelvic bone ossification

We observed modest hip joint abnormalities in *Trps1*$^{\Delta Enh1/-}$, *Trps1*$^{\Delta Enh2/-}$, *Trps1*$^{\Delta Enh3/}$ mice. It has been established that a high proportion of patients with TRPS experience early onset coxarthritis [2]. Although *Trps1*$^{-/-}$ mice have been used to investigate the skeletal pathologies of TRPS, hip joint formation in this mutant strain has not yet been examined in detail. Therefore, we set out to address this issue in *Trps1*$^{-/-}$ mice (Fig. 2). *Trps1* was expressed in the hip joint region between the developing acetabulum of the coxa and the femoral head at E12.5 (Fig. 2A1). The cartilage primordia of both coxa and femur, which were characterized by Sox9 expression, were normally formed in WT (Fig. 2A2) and *Trps1*$^{-/-}$ (Fig. 2A3) embryos. At E15.5, the pelvic bone (os coxa), femur, tibia, and fibula containing mineralized primary ossification centers were observed in WT, *Trps1*$^{+/-}$, and *Trps1*$^{-/-}$ embryos (Figs. 2B and 2C, and data not shown). Although pelvic bone exhibited ossification in the iliac portion and length of pelvis was similar in WT and *Trps1*$^{-/-}$

For Peer Review

embryos, mineralized region was limited in *Trps1*$^{-/-}$ embryos (arrowheads in Fig. 2C). At E17.5, although primary ossification of the ilium, ischium, and pubis was initiated in WT, *Trps1*$^{+/-}$, and *Trps1*$^{-/-}$ embryos, the length of pelvic bone was shorter in *Trps1*$^{-/-}$ embryos (Figs. 2D, 2E). Furthermore, the lateral view of the pelvic bone revealed that the angle between the anterior (ilium) and posterior (ischium and pubis) portion is sharply bent in *Trps1*$^{-/-}$ embryos compared to WT and *Trps1*$^{+/-}$ (Fig. 2F, 2G). Thus, the global lack of *Trps1* results in developmental abnormalities in mineralization, growth, and morphological curvature of the coxa.

3. *Trps1*$^{\Delta int/\Delta int}$ mice lacking both Enh2 and Enh3 displayed growth delays and skeletal defects

To examine the potential cooperative effects of Enh2 and Enh3 on *Trps1* expression and skeletal development, we generated mutant mice lacking a 20 kb region within the first intron of *Trps1*, which contains both Enh2 and Enh3, by genome editing (Suppl. Fig. 1). Homozygous intron knockout mice (referred to as *Trps1*$^{\Delta int/\Delta int}$ mice hereafter) survived postnatally and were fertile, even in *Trps1*$^{\Delta int/\Delta int}$ male and female mating pairs. The number of *Trps1*$^{\Delta int/\Delta int}$ mice at postnatal 3 weeks was slightly lower than expected, thus suggesting that some *Trps1*$^{\Delta int/\Delta int}$ mice died before weaning (Suppl. Fig. 4A). *Trps1*$^{\Delta int/\Delta int}$

For Peer Review

mice exhibited significantly lower body weight during postnatal periods (statistically significant through postnatal weeks 3 to 9) compared to that of the WT or *Trps1*$^{\Delta int/+}$ mice (Suppl. Fig. 4B). When expression level of *Trps1* was examined in several organs of the early postnatal pups (Suppl. Fig. 4C), *Trps1* levels were significantly reduced in the kidney, pelvis, scapula, and rib cartilage of *Trps1*$^{\Delta int/\Delta int}$ mice (Suppl. Fig. 4C). The reduction in *Trps1* expression was mild in the pelvic and rib cartilage. In contrast, there were no significant changes in *Trps1* expression in the heart or skin, and vibrissa follicle of *Trps1*$^{\Delta int/\Delta int}$ mice. *Trps1* expression was also assessed in cultured costal chondrocytes prepared from the WT, *Trps1*$^{\Delta Enh2/\Delta Enh2}$, *Trps1*$^{\Delta Enh3/\Delta Enh3}$, and *Trps1*$^{\Delta int/\Delta int}$ mice (Suppl. Fig. 4D). In *Trps1*$^{\Delta int/\Delta int}$ chondrocytes, the *Trps1* expression level was significantly decreased to approximately 40% of the WT; the level was also significantly reduced in *Trps1*$^{\Delta Enh3/\Delta Enh3}$ chondrocytes (Suppl. Fig. 3D), whereas the reduction was mild compared to that in the cells of *Trps1*$^{\Delta int/\Delta int}$ pups.

We next analyzed the skeletons of newborn *Trps1*$^{\Delta int/\Delta int}$ pups (Suppl. Figs. 4). Compared to the control pups, *Trps1*$^{\Delta int/\Delta int}$ pups showed no obvious defects in their body size (Suppl. Fig. 5A). The morphologies of the head and neck skeletons (Suppl. Figs. 5B-5G), the mineralization of the vertebral body and arches (Suppl. Figs. 5H-5M), the morphogenesis and ossification of the forelimb morphogenesis and ossification were

For Peer Review

normal in these mutants (Suppl. Figs. 5N-5Q), the gross appearance of the hind limb was also similar between the control and mutants (Suppl. Figs. 5R-5U). However, *Trps1*$^{\Delta int/\Delta int}$ pups displayed 14% reduction in the size of the pelvis (Suppl. Fig. 5T; P<0.001) and a tendency of reduction in the length of the femur (Fig. 5U).

4. Adult *Trps1*$^{\Delta int/\Delta int}$ mice display developmental delays in formation of pelvic girdle and secondary ossification center

The defects of the pelvis and femur in *Trps1*$^{\Delta int/\Delta int}$ mice led us to focus on their hip joints. They survived to the mature stage, and this allowed us to examine the postnatal structure of the hip joint in these mutants. At 1-month postnatal, 3D-CT images showed well-mineralized hip bones in both control (Fig. 3A) and *Trps1*$^{\Delta int/\Delta int}$ mice (Fig. 3B). The cartilaginous ilio-pubic junction appeared to be wider in *Trps1*$^{\Delta int/\Delta int}$ mutants at this developmental stage (arrowheads in Fig. 3B). Histological analysis revealed that the cartilaginous remnants between the ilio-pubic junctions were more abundant in *Trps1*$^{\Delta int/\Delta int}$ mice (Fig. 3D), whereas they were in the well-defined narrow cartilaginous domains in the control mice (Fig. 3C). At 3-months postnatal, the cartilaginous ilio-pubic junctional domain were replaced by mature bone in both control (Fig. 3E) and *Trps1*$^{\Delta int/\Delta int}$ mice (Fig. 3F). However, 3D-CT images showed that the psoas valley of

For Peer Review

Trps1$^{\Delta int/\Delta int}$ mice (arrowheads in Fig. 3H) was more deeply invaginated than that of control mice (Fig. 3G), thus resulting in increased psoas valley depth in the mutants (Figs. 3I and 3J).

The formation of a secondary ossification center (SOC) is crucial for reducing the physical impact of the cartilaginous epiphyseal growth plate [32]. On day 10 postnatal, in *Trps1*$^{\Delta int/\Delta int}$ mice (Fig. 3L) the initiation of SOC formation was delayed compared to that in control mice (Fig. 3K); both vascular canal invasion and hypertrophic differentiation of the epiphyseal resting chondrocytes were delayed in *Trps1*$^{\Delta int/\Delta int}$ mice. In the first postnatal month when the SOC is usually fully formed, the SOC was formed in both the control (Figs. 3M and 3M') and the *Trps1*$^{\Delta int/\Delta int}$ mice (Figs. 3Q and 3Q'). Osteoblasts expressing *Col1a1* were observed in the SOC of the control (Fig. 3N) and *Trps1*$^{\Delta int/\Delta int}$ mice (Fig. 3R). However, cartilaginous remnants stained for toluidine blue (see red arrowheads in Fig. 3Q' compared to Fig. 3M') were detected in the *Trps1*$^{\Delta int/\Delta int}$ SOC; cells in the remnants expressed *Col2a1* (see red arrows in Fig. 3S compared to Fig. 3O) but not *Col10a1* (Figs. 3P and 3T). Thus, adult *Trps1*$^{\Delta int/\Delta int}$ mice exhibited developmental delays in coxa and SOC formation. Furthermore, *Trps1*$^{\Delta int/\Delta int}$ mice displayed an increase in the psoas valley depth, possibly resulting in regional under-coverage of the femoral head within the acetabulum.

For Peer Review

5. *Trps1*$^{\Delta int/-}$ mice display reduced survival rates, severe growth defects, acetabular dysplasia, and patella dislocation.

Trps1$^{\Delta int/-}$ mice were generated by mating *Trps1*$^{\Delta int}$ mice with *Trps1*$^{+/-}$ mice. Timed mating embryos were collected at E17.5. *Trps1*$^{\Delta int/-}$ embryos were visually indistinguishable from WT embryos (Suppl. Fig. 6A). However, on postnatal day 5 (Suppl. Fig. 6B) or at later mature stages (Suppl. Fig. 6C), *Trps1*$^{\Delta int/-}$ mice were significantly smaller. Also, the number of the *Trps1*$^{\Delta int/-}$ animals surviving to the weanling stage were extremely low compared to other genotypes (Suppl. Fig. 6D).

We first analyzed skeletal development of *Trps1*$^{\Delta int/-}$ embryos at E18.5 (Suppl. Figs. 6E-6Q). As described above, body size was comparable between control and *Trps1*$^{\Delta int/-}$ embryos (Suppl. Fig. 6E). Control and *Trps1*$^{\Delta int/-}$ embryos demonstrated no obvious difference in craniofacial skeletons (Suppl. Figs. 6F-6I, 6L, and 6M), appendicular skeletons (Suppl. Figs. 6J, 6K), sternum (Suppl. Figs. 6N and 6O), and rib cage (Suppl. Figs. 6P and 6Q). Thus, despite the postnatal growth defects of *Trps1*$^{\Delta int/-}$ mice, their embryonic skeletal defects were negligible small.

We analyzed *Trps1* expression in tissues harvested from rib, knee, vertebral cartilage and kidney from postnatal day 0 pups (Suppl. Figs. 7A-7D). The expression level of *Trps1*

For Peer Review

showed increased tendency in *Trps1*$^{+/-}$ mice, while *Trps1* expression was not significantly reduced in *Trps1*$^{\Delta int1/-}$ tissues obtained from rib (Suppl. Fig. 7A), knee (Suppl. Fig. 7B), and vertebral cartilage (Suppl. Fig. 7C). In contrast, *Trps1* expression in *Trps1*$^{\Delta int/-}$ neonate kidney showed significant reduction (Suppl. Fig. 7D).

We obtained two surviving *Trps1*$^{\Delta int/-}$ mice at the weaning stage (Suppl. Fig. 6D). These mice survived for more than 3 months postnatally (samples were collected at 3- and 6-months postnatally). They were both female, but neither gave birth to pups. Macroscopic anatomy (Figs. 4A and 4B) and 3D-CT analysis (Figs. 4C and 4D) revealed a deeply invaginated psoas valley together with severe under-coverage of the femoral head within the acetabulum. Histologically, the cartilaginous ilio-pubic junction remained even in 3-month-old *Trps1*$^{\Delta int/-}$ mice (Figs. 4F and 4H), but not in the control mice (Figs. 4E and 4G).

3D-CT analysis also revealed other skeletal pathologies of the *Trps1*$^{\Delta int/-}$ mice, including the medial dislocation of the patella (Figs. 4I and 4J; observed in four out of four knees), reduced development of the fabella that is a sesamoid bone embedded in the lateral head of the gastrocnemius muscle (Figs.4K and 4L; observed in four out of four knees), shallow and flattened trochlear groove (Figs. 4J and 4L; observed in four out of four knees), and reduced area of the SOC domain (Figs. 4M and 4N). Given that the patellar dislocation

For Peer Review

was not observed in perinatal *Trps1*$^{\Delta int/-}$ pups (Fig.4O), dislocation was likely to occur postnatally in the mutants. Histologically, *Trps1*$^{\Delta int/-}$ mice showed not just the reduced size of the SOC, but also the presence of cartilaginous remnant even at 3-months postnatal (Figs. 4P-4S). Thus, *Trps1*$^{\Delta int/-}$ mice displayed more severe pathologies than *Trps1*$^{\Delta int/\Delta int}$ mice.

For Peer Review

Discussion

The pelvic girdle functions as a load-bearing structure in both bipedal and quadrupedal animals. The precise morphogenesis and alignment of the pelvis, femur, and other joint structures are crucial for tolerating various types and times of hip joint movement without friction. Compared to the knowledge of genes involved in fore- and hindlimb development, much less is known regarding the genetic regulation of pelvic girdle development. Here, we demonstrate that the transcription factor Trps1 is important for normal pelvic development. We observed that the size relationship between the femoral head and acetabulum was altered when the expression of *Trps1* was low. In particular, the development of the pubic bone was mostly affected, and the acetabulum of the ilio-pubic junction exhibited under-coverage of the femoral head. These observations reinforce the indispensable role of Trps1 in the normal pelvic girdle morphogenesis. The psoas valley is an anterior depression located at the acetabular rim and coincides with a site commonly associated with acetabular labral pathology [33]. The invagination of the psoas valley was severely affected in $Trps1^{\Delta int/\Delta int}$ and surviving $Trps1^{\Delta int/-}$ mice. This phenotype may partly explain the etiology of frequently observed hip dysplasia and early onset coxarthrosis in patients with TRPS.

For Peer Review

1. Postnatal skeletal dysplasia by deletion of potential regulatory elements in the first intron of murine *Trps1* gene

Our understanding of the transcriptional regulation of *Trps1* expression is still limited. Advances in high-throughput sequencing have revealed chromatin accessibility, chromatin modifications, and transcription factor binding sites [34]. The functional significance of computational data from ATAC-seq and ChIP-seq needs to be verified experimentally, most ideally by *in vivo* strategies. We identified several enhancer candidates in the murine *Trps1* gene region that were mostly regionalized to the 5' side of the first intron. This genomic region is well conserved in mammals (opossums and humans), whereas the chicken sequence is much less conserved. To examine their biological significance, we deleted the identified sequences using genome editing approaches in mice. Furthermore, we generated compound heterozygous mice in which the enhancers were deleted with a disrupted *Trps1* gene in another allele.

Chondrocytes derived from $Trps1^{\Delta int/\Delta int}$ mice exhibited an approximately 60% reduction in *Trps1* expression compared to the WT cells. Interestingly, chondrocytes harvested from $Trps1^{\Delta Enh3/\Delta Enh3}$ mice also exhibited reduced *Trps1* expression (and $Trps1^{\Delta Enh2/\Delta Enh2}$ exhibited a tendency for reduction) compared to the WT cells. This observation indicated that there were at least two independent enhancers, which regulates *Trps1* expression,

For Peer Review

within the first intron of the *Trps1* gene.

The presence of introns in the gene body is known to play various roles in the cell, where 1) they upregulate transcription through intron-mediated enhancement of transcription [35], 2) they increase proteomic complexity through alternative splicing [36], and 3) they alleviate the genotoxic R-loop formation that appears during the transcriptional process [37]. Introns can regulate gene expression, where they reside both at the level of transcription [38] and post-transcriptionally [39; 40]. Recent evidence suggests that many key cis-regulatory regions are located in the introns of their target genes [41]; especially, tissue-specific enhancers are highly enriched in intronic regions, regulating the expression of genes that function in tissue-specific manners [42]. Furthermore, an intergenic-to-intronic active enhancer continuum is observed during the transition from developmental to adult stages; the most differentiated tissues tend to exhibit higher rates of intronic enhancers [42]. Given these, the genomic regions that we identified as enhancer candidates are possibly involved in tissue-specific expression and functions of *Trps1*. Skeletal phenotypes of our enhancer deleted mice further support this notion.

Individual deletions of Enh1, Enh2, and Enh3 caused subtle phenotypes in mice, suggesting that each of the single enhancer is functionally dispensable for normal skeletal development or they have functional redundancy. Importantly, these mutants

For Peer Review

displayed a mildly deformed acetabulum when the *Trps1* gene dosage was further reduced by deletion of one allele of *Trps1*. This result raises the possibility that each enhancer contributes to hip joint maturation when the genetic robustness of *Trps1* expression is reduced. This idea was supported by the observation that more severe acetabular defects were present when Enh2 and Enh3 were simultaneously deleted. The coincidence of the defective anatomical site observed in different *Trps1* enhancer mutant strains and the difference in the severities observed strongly indicate that normal acetabular morphogenesis depends upon a sufficient *Trps1* gene dose.

Trps1$^{\Delta int/-}$ mice display the most severe growth defects among the mice we tested; however, these defects became apparent postnatally. Recent evidence suggests that postnatal skeletal growth is driven by the activation of the stem cell niche that appears in synchronization with the maturation of SOC [43; 44]. The postnatal growth defects and defective SOC formation in *Trps1*$^{\Delta int/-}$ mice suggest that the diminished chondrocyte stem cell population may be the cause of their gradual pronounced shortening of body length.

2. Skeletal pathologies in TRPS patients and TRPS mouse models

Greater than 50% of patients with TRPS exhibit developmental dysplasia of the hip [2; 13]. These malformations include coxa plana (resembling the femoral head morphology

For Peer Review

in Perthes disease), coxa magna (relative enlargement of the femoral head), and coxa vara (reduction of the femoral neck shaft angle). Possibly due to these abnormal developments, older patients with TRPS display hip abnormalities associated with degenerative coxarthrosis. Although these reports suggest important roles for Trps1 in hip joint development, they have not been investigated by mouse genetics to date. The present study addressed this issue. Conventional *Trps1*$^{-/-}$ mice exhibited a reduction in the size of the ilium, ischium, and pubis. The width of the pelvic floor was narrower, and the subpubic angle was more acute in *Trps1*$^{-/-}$ embryos. As the pubic symphysis is normally observed in *Trps1*$^{-/-}$ mice, the short anterior-posterior length of the pelvis appears to be compensated for by the bending of the pelvis at the ilium and ischium/pubis border (Suppl. Fig. 5).

As the pelvis and femur phenotypes of *Trps1*$^{\Delta int/\Delta int}$ mice were similar to those of *Trps1*$^{-/-}$ mice at the perinatal stage, we examined the hip joint morphology of *Trps1*$^{\Delta int/\Delta int}$ mice at the adult stage. The pubic bone element was particularly affected in *Trps1*$^{\Delta int/\Delta int}$ mice, and consequently the acetabulum of the pubic bone region was poorly formed, ultimately resulting in undercoverage of the femoral heads. These morphological changes often lead to altered joint load and motion, thus causing the onset of degenerative joint pathologies [45; 46]. These conclusions are further supported by reports correlating an increased risk

For Peer Review

of osteoarthritis with morphological deformities of the proximal femur and acetabulum [47; 48].

Trps1$^{\Delta int/-}$ mice displayed patella formation in the normal position; however, in adult mice that survived to the mature stage, medial patellar dislocation was observed in all examined knees. Significantly, it has been reported that some patients with TRPS display an abnormal patella with recurrent dislocation [49]. The patella is the largest sesamoid bone embedded in the quadriceps tendon and facilitates musculoskeletal function. Development of the patella was originally thought to occur inside the tendons in response to mechanical signals from the attaching muscles [50]; however, it is now established that in the mouse embryo, the patella initially develops as a bony process at the anterodistal surface of the femur from Sox9 and Scleraxis double-positive progenitor cells and separates from the distal femur via Gdf5-positive joint formation [51]. Postnatally, the patella plays a crucial role in knee mechanics and stability and facilitates hind limb function and locomotion [52]. The patella increases the distance between the quadriceps and knee, and thereby increasing the moment arm of the muscle and enhancing its extension force by 50% [53]. The normal patellar position in newborn *Trps1*$^{\Delta int/-}$ pups indicates that patella development initiates normally at the correct location, and the dislocation occurred postnatally in the mutants. The patella stability

For Peer Review

involves a balance between the stabilizing patellofemoral ligaments, the osteoarticular surface, the position of the patella (high riding patella; patella alta), decreased depth or flattened trochlear groove, and the muscular actions of the quadriceps muscles [54]. 3D-CT images of the distal femur of the *Trps1*$^{\Delta int/-}$ mice indicate the flattened surface at the femoral trochlear groove at 3- and 6-months-of-age. The medial and lateral facets of the groove are not obvious but rather exhibit convexity, ultimately resulting in apparent trochlear dysplasia [55]. Interestingly, the medial fabella, a sesamoid bone embedded in the medial head of the gastrocnemius muscle, exhibited a severe reduction in size. It is important to note that in quadrupedal mammals, the fabella is believed to play a role very similar to that of the patella in redirecting the extension forces of the knee joint from one point to another [56]. The exact causes of the flattened femoral trochlear groove and reduced medial fabella size are not clear. Skin and joint laxity is a characteristic feature of patients with TRPS. These features of TRPS have been described as symptoms that are similar to those observed in patients with Ehlers-Danlos syndrome. Importantly, a mouse model of Ehlers-Danlos syndrome exhibited severe growth retardation, delays in SOC formation, and patellar dislocation, all of which were observed in *Trps1*$^{\Delta int/-}$ mice [57].

For Peer Review

3. The *Trps1*$^{\Delta int/\Delta int}$ mouse strain as a novel TRPS disease model for postnatal studies.

The etiologies of TRPS have been investigated using several animal models of TRPS. Most of these studies were performed using homozygous knockout mice. Although they are useful, they possess significant limitations due to their early postnatal lethality. Patients with TRPS exhibit various postnatal diseases. These conditions include skeletal dysplasia, coxarthrosis, and progressive short stature [2]. Our novel *Trps1*$^{\Delta int/\Delta int}$ mouse strain could partially overcome this limitation, contributing to the postnatal studies of TRPS pathologies.

For Peer Review

Materials and Methods

1. ATAC-seq and ChIP-seq of mouse costal chondrocytes.

Assays for transposase-accessible chromatin using high-throughput sequencing (ATAC-seq) [58] was performed using costal chondrocytes isolated from neonatal mouse ribs [59]. Approximately 50,000 cells were lysed using lysis buffer (10 mM Tris-HCl, pH 7.4, 10 mM NaCl, 3 mM $MgCl_2$, and 0.1% IGEPAL CA-630) to release the nuclei and then treated with Tn5 transposase (Illumina #FC121-1030) at 37°C for 30 minutes. The adaptors were ligated and amplified using polymerase chain reaction (PCR) for high-throughput sequencing. Paired-end sequencing (100 bp) was performed using an Illumina HiSeq platform at the Osaka University Research Institute for Microbial Diseases NGS Core Facility. Qualified sequencing reads were aligned to the reference genome (mm9) using Bowtie 2 (ver. 2.4.4) [60], and MACS2 was used for peak calling [61]. Two biological replicates were analyzed for ATAC-seq. Chromatin immunoprecipitation followed by sequencing (ChIP-seq) was performed using antibodies against histone modifications [62]. Primary chondrocytes were crosslinked with 1% formaldehyde for 5 min. Crosslinking was quenched with 1 M glycine for 5 min. Cells were lysed and chromatin was sonicated with Covaris M220. Fragmented DNA was immunoprecipitated using an antibody against acetylated H3 lysine 27 (H3K27ac) (Cell Signaling Technology

For Peer Review

(CST) #8173, 2 μg per reaction) or against demethylated H3 lysine 4 (H3K4me2) (CST, #9725, 2 μg per reaction). H3K27ac is associated with active enhancer regions, while H3K4me2 is predominantly enriched around the functional cis-regulatory elements as well as transcription start sites (TSS) [63]. All immunoprecipitation was performed for 4 hours at 4°C. ChIP samples were washed, eluted at 65°C for 30min, and reverse crosslinked at 65°C overnight. DNA was purified using DNA purification spin columns. Library preparation, sequencing, and peak calling were performed as described above. ATAC-seq and ChIP-seq data have been deposited in the NCBI Gene Expression Omnibus with the accession code GSE237889 (https://www.ncbi.nlm.nih.gov/geo/query/acc.cgi?acc=GSE237889).

2. Luciferase assays

The enhancer 2 (Enh2; 2,981 bp) and enhancer 3 (Enh3; 5,370 bp) genomic fragments were amplified using a high-fidelity KODFX DNA polymerase (TOYOBO, Osaka, Japan) by the primer sequences listed in Table 1. The A-tailed fragments were subcloned into the pTA2 vector (TOYOBO). The inserts were released and subcloned into the pGL3-promoter vector (Promega) to generate Enh2-Luciferase and Enh3-Luciferase constructs. The Enh3 fragment was inserted into the Enh2-Luciferase clone to generate an Enh2-Enh3-Luciferase construct. Firefly Luciferase vectors and pTK-Renilla luciferase vector

For Peer Review

(Promega) were transfected into ATDC5 chondrocytic cell line seeded onto 12-well culture plates [64; 65] with ScreenFect A (Fujifilm, Osaka, Japan) for 6 h. The cells were rinsed once with phosphate buffered saline (PBS) and then cultured in DMEM/F-12 media (Sigma) supplemented with 10% fetal bovine serum (FBS). After cultured for an additional 40 h, the cells were lysed with 200 μl of luciferase lysis buffer (Promega). Luciferase measurements and normalization were performed as described previously [66; 67]. The experiments were performed in triplicate and performed at least three times, and representative data are presented in the figures.

3. Animals

Conventional *Trps1* knockout mouse strain (*Trps1*$^{-/-}$ mice) has been described previously [5; 8]. *Trps1* enhancer-deleted strains were generated by CRISPR/Cas9 genome editing. ΔEnh1 strain was generated by the deletion of the enhancer 1 (Enh1) sequence, which is located upstream of *Trps1* TSS [31]. Enh2 and Enh3 are located in the first intron of the *Trps1* gene; approximately 3 kb (Enh2), 4 kb (Enh3), and 20 kb genomic regions containing both of the enhancers were deleted in ΔEnh2, ΔEnh3, and Δint strains, respectively. The guide RNA sequences used for genome editing are listed in Table 1. crRNA, tracrRNA, and the Cas9 protein complex were electroporated into fertilized eggs (C57BL/6J) and cultured *in vitro* until the two-cell stage. Eggs were implanted into the

For Peer Review

fallopian tubes of pseudo-pregnant female mice. F0 mice with successful deletions were initially mated with C57BL/6J wild-type (WT) mice (Japan SLC, Inc., Shizuoka, Japan) for germline transmission. Non-mosaic heterozygotes of F1 males and females were used for breeding. To generate *Trps1* double heterozygotes including *Trps1*$^{\Delta int/-}$ mice, we crossed *Trps1* enhancer-deleted strain with conventional *Trps1* heterozygous knockout strain. Genotyping was performed using the genomic DNA purified from tail clips or skin tissue. Primer used for genotyping are listed in Table 2.

Body weight was measured every week after weaning until week 9. For embryonic stage sample preparation, noon of the day the vaginal plug appeared was considered as embryonic day (E) 0.5. Pregnant female mice were humanely euthanized, and embryos were collected by C-section. All animal experiments were approved by the Animal Experiment Committee of the Osaka University Graduate School of Dentistry (Animal Protocol #29-016-0). Experimental procedures were performed according to the Association for Assessment and Accreditation of Laboratory Animal Care International and local guidelines. The rooms were maintained at 22 to 26 degrees under 12 h light/dark cycle.

4. Skeletal analysis

Alizarin red and alcian blue staining of bone and cartilage was performed as previously

For Peer Review

described [68]. Three-dimensional micro-computed tomography (3D-CT) images of the pelvic region were captured by R-mCT2 (Rigaku, Tokyo, Japan) at Field of view (FOV) 20 at 90V and 160μA. Images were created using three-dimensional reconstruction imaging software (TRI/ 3D-BON; RATOC System Engineering Co., Ltd., Tokyo, Japan). The psoas valley depth was measured according to a previous report [69]. Briefly, a straight line passing through the upper and lower hip labra was drawn. A line perpendicular to and crossing the center of the femoral head was drawn. The lengths of the psoas valleys depth were measured using the ImageJ software. As there could be sex-specific variations in pelvic girdle morphology, we used only male mice for the postnatal study. Sex was not determined for the embryonic stage samples used in this study.

4. Total RNA isolation from primary costal chondrocytes and reverse transcription-quantitative PCR (RT-qPCR).

Postnatal day 3 (PNd3) pups were humanely euthanized by injecting them with an overdose of anesthetic drugs, and various tissues or organs were dissected in cold PBS under a stereoscopic microscope. Each tissue and organ was stored separately in 350 μl buffer RLT (Qiagen, Hilden, Germany) supplemented with beta-mercaptoethanol. Total RNA was prepared using an RNeasy Plus kit (Qiagen) according to the manufacturer's

For Peer Review

instructions. Samples obtained from both WT and *Trps1*$^{\Delta int/\Delta int}$ animals were homogenized and subjected to the column purification processes. WT, *Trps1*$^{\Delta Enh2/\Delta Enh2}$, *Trps1*$^{\Delta Enh3/\Delta Enh3}$, and *Trps1*$^{\Delta int/\Delta int}$ were used for preparation of the neonatal costal chondrocytes. Cells were harvested as described previously [59]. The cells were cultured in DMEM supplemented with 10% FBS and antibiotics. Cells from passage two were used for qPCR analysis. Purified total RNA (1 μg) was reverse-transcribed into cDNA using ReverTra Ace (TOYOBO). THUNDERBIRD SYBR qPCR mix (TOYOBO) was used for real-time PCR on a 20 μl reaction scale. A MiniOpticon qPCR apparatus equipped with CFX managing software (Bio-Rad Laboratories, Berkeley, CA, USA) was used for reaction and data acquisition as described previously [70]. The primers used for real-time PCR were 5'-CAG CTC CCA AGA GCA GAC AAA-3' and 5'-GTC AGG CAA TTG GCA CAA AAA-3' for *Trps1*, and the primer sequence for *Hprt1* has been described previously [71].

3. *In situ* hybridization and immunohistochemistry

Sectional *in situ* hybridization was performed as previously described [5]. Transverse cryo-sections of E12.5 embryos were prepared at thickness of 14 microns. Sense and antisense *Trps1* cRNA probes were synthesized using the NM_032000.2 nt.412-1291 sequence as a template. Immunohistochemistry was performed on transverse cryo-

For Peer Review

sections of E12.5 wildtype and *Trps1*$^{-/-}$ embryos using anti-Sox9 rabbit monoclonal antibody (1:400 #D8G8H, CST, Danvers MA). Endogenous peroxidase activity was inhibited by 0.3% H_2O_2 for 15 min at RT. Biotinylated anti-rabbit IgG (4 μg/ml Vector Laboratories, Burlingame, CA) and HRP-conjugated streptavidin (2 μg/ml; Abcam, Cambridge, UK) were used for the following reactions. Color development was performed using 3,3'-Diaminobenzidine with nickel enhancement. Normal rabbit IgG (CST) was used instead of the primary antibody as a negative control. The stained sections were then dehydrated and covered with coverslips. Postnatal animals were fixed by perfusion under deep anesthesia. The hindlimbs were further fixed in 4% paraformaldehyde for more than 16 hours at 4 degrees. Then, the samples were decalcified in 10% ethylenediamine tetraacetic acid (EDTA) for 10 to 14 days at 4 degrees Celsius. The decalcified samples were dehydrated, embedded in paraffin, and then sectioned at a 4-micron thickness. Stained images were captured using an Axioskop 2 plus equipped with an Axiocam 208 (Carl Zeiss Microscopy, Jena, Germany) or BZ-X800 with appropriate software (Keyence).

4. Statistical analysis.

The results are expressed as the means ± standard deviation (SD). The mean values of two samples were compared using Student's *t-test*. Statistical significance was set at *P*

For Peer Review

< 0.05. Multiple comparison of more than three samples were analyzed by one-way analysis of variance (ANOVA), followed by Tukey's post-hoc test using GraphPad Prism8 software. At least three animals per each genotype were used for all the analysis.

For Peer Review

Acknowledgements

This work was supported by Grants-in-Aid for Scientific Research from MEXT to MA (17K11611, 22K06295), JSPS KAKENHI JP16H06276 (AdAMS) to MA, and the Takeda Science Foundation for SI. The authors acknowledge Dr. Yasuteru Muragaki for sharing the *Trps1* knockout strain; Dr. Ryouji Yao, Dr. Hiroshi Takano, Dr. Hitomi Yamanaka, and Dr. Masahito Ikawa for their help with mouse generation; and Ms. Mariko Kasai for the technical assistance.

Declaration of interests

None.

Author contributions

N.S., S.O., M.A. conceived of the study, T.I., S.A., S.O., M.A. supervised the work, N.S., K.H., S.I., S.O., M.A. designed the experiments, N.S., C.I-Y., Y.I., R.K., K.H., S.O., M.A. performed the experiments and analyzed results, N.S., S.O., M.A. wrote the manuscript with input from all authors.

For Peer Review

References

1. Momeni, P., Glockner, G., Schmidt, O. et al. Mutations in a new gene, encoding a zinc-finger protein, cause tricho-rhino-phalangeal syndrome type I. *Nat Genet* 2000;**24**:71-74.

2. Ludecke, H.J., Schaper, J., Meinecke, P. et al. Genotypic and phenotypic spectrum in tricho-rhino-phalangeal syndrome types I and III. *Am J Hum Genet* 2001;**68**:81-91.

3. Le Saout, J., Lefevre, C., Kerboul, B. et al. Osteochondritis of the hip and the tricho-rhino-phalangeal syndrome. *Ann de Chirurgie* 1984;**38**:357-362.

4. Itoh, S., Kanno, S., Gai, Z., et al. Trps1 plays a pivotal role downstream of Gdf5 signaling in promoting chondrogenesis and apoptosis of ATDC5 cells. *Genes Cells* 2008;**13**:355-363.

5. Michikami, I., Fukushi, T., Honma, S. et al. Trps1 is necessary for normal temporomandibular joint development. *Cell Tis Res* 2012;**348**:131-140.

6. Napierala, D., Sam, K., Morello, R.et al. Uncoupling of chondrocyte differentiation and perichondrial mineralization underlies the skeletal dysplasia in tricho-rhino-phalangeal syndrome. *Hum Mol Genet* 2008;**17**:2244-2254.

7. Napierala, D., Sun, Y., Maciejewska, I.et al. Transcriptional repression of the Dspp gene leads to dentinogenesis imperfecta phenotype in Col1a1-Trps1 transgenic mice. *J Bone Min Res* 2012;**27**:1735-1745.

For Peer Review

8. Suemoto, H., Muragaki, Y., Nishioka, K. et al. Trps1 regulates proliferation and apoptosis of chondrocytes through Stat3 signaling. *Dev Biol* 2007;**312**:572-581.

9. Kanno, S., Gui, T., Itoh, S.et al. Aberrant expression of the P2 promoter-specific transcript Runx1 in epiphyseal cartilage of Trps1-null mice. *Exp Mol Pathol* 2011;**90**:143-148.

10. Nishioka, K., Itoh, S., Suemoto, H. et al. Trps1 deficiency enlarges the proliferative zone of growth plate cartilage by upregulation of Pthrp. *Bone* 2008;**43**:64-71.

11. Wuelling, M., Kaiser, F.J., Buelens, L.A. et al. Trps1, a regulator of chondrocyte proliferation and differentiation, interacts with the activator form of Gli3. *Dev Biol* 2009;**328**:40-53.

12. Wuelling, M., Schneider, S., Schrother, V.A. et al. Wnt5a is a transcriptional target of Gli3 and Trps1 at the onset of chondrocyte hypertrophy. *Dev Biol* 2020;**457**:104-118.

13. Maas, S.M., Shaw, A.C., Bikker, H. et al. Phenotype and genotype in 103 patients with tricho-rhino-phalangeal syndrome. *Eur J Med Genet* 2015;**58**:279-292.

14. Fontaine, G., Maroteaux, P., Farriaux, J.P. et al. The tricho-rhino-phalangeal syndrome. *Arch Fr Pediatr* 1970;**27**:635-647.

15. Beals, R.K. Tricho-rhino-phalangeal dysplasia. Report of a kindred. *J Bone Joint Surg Am* 1973;**55**:821-826.

For Peer Review

16. Felman, A.H., Frias, J.L. The trichorhinophalangeal syndrome: study of 16 patients in one family. *AJR Am J Roent* 1977;**129**:631-638.

17. Peltola, J., Kuokkanen, K. Tricho-rhino-phalangeal syndrome in five successive generations: Report on a family in Finland. *Acta Dermato-Vener* 1978;**58**:65-68.

18. Howell, C.J., Wynne-Davies, R. The tricho-rhino-phalangeal syndrome. A report of 14 cases in 7 kindreds. *J Bone Joint Surg Br* 1986;**68**:311-314.

19. Don, E.K., Currie, P.D., Cole, N.J. The evolutionary history of the development of the pelvic fin/hindlimb. *J Anat* 2013;**222**:114-133.

20. Yano, T., and Tamura, K. The making of differences between fins and limbs. *J Anat* 2013;**222**:100-113.

21. Malashichev, Y., Borkhvardt, V., Christ, B. et al. Differential regulation of avian pelvic girdle development by the limb field ectoderm. *Anat Embryol* 2005;**210**:187-197.

22. Delaere, O., Kok, V., Nyssen-Behets, C. et al. Ossification of the human fetal ilium. *Acta Anat* 1992;**143**:330-334.

23. Ponseti, I.V. Growth and development of the acetabulum in the normal child. Anatomical, histological, and roentgenographic studies. *J Bone Joint Surg Am* 1978;**60**:575-585.

24. Harrison, T.J. The influence of the femoral head on pelvic growth and acetabular

For Peer Review

652 form in the rat. *J Anat* 1961;**95**:12-24.

653 25. Harris-Hayes, M., Royer, N.K. Relationship of acetabular dysplasia and
654 femoroacetabular impingement to hip osteoarthritis: a focused review. PM & R : *J Inj*
655 *Funct Rehab* 2011;**3**:1055-1067 e1051.

656 26. Anderson, F.A., Jr., Huang, W., Friedman, R.J. et al. Prevention of venous
657 thromboembolism after hip or knee arthroplasty: findings from a 2008 survey of US
658 orthopedic surgeons. *J Arthro* 2012;**27**:659-666 e655.

659 27. Diesel, C.V., Ribeiro, T.A., Scheidt, R.B. et al. The prevalence of femoroacetabular
660 impingement in radiographs of asymptomatic subjects: a cross-sectional study. *J Clin*
661 *Exp Res Hip Pathol Ther* 2015;**25**:258-263.

662 28. Storer, S.K., Skaggs, D.L. Developmental dysplasia of the hip. *Am Fam Phys*
663 2006;**74**:1310-1316.

664 29. McWilliams, D.F., Doherty, S.A., Jenkins, W.D. et al. Mild acetabular dysplasia and
665 risk of osteoarthritis of the hip: a case-control study. *Annals Rheum Dis* 2010;**69**:1774-
666 1778.

667 30. Jacobsen, S., Sonne-Holm, S. Hip dysplasia: a significant risk factor for the
668 development of hip osteoarthritis. A cross-sectional survey. *Rheumatology* 2005;**44**:211-
669 218.

For Peer Review

670 31. Nomir, A.G., Takeuchi, Y., Fujikawa, J. et al. Fate mapping of Trps1 daughter cells
671 during cardiac development using novel Trps1-Cre mice. *Genesis* 2016;**54**:379-388.
672 32. Xie, M., Gol'din, P., Herdina, A.N. et al. Secondary ossification center induces and
673 protects growth plate structure. *eLife* 2020;9.
674 33. Kopydlowski, N.J., Tannenbaum, E.P., Smith, M.V. et al. Characterization of Human
675 Anterosuperior Acetabular Depression in Correlation With Labral Tears. *Orthop J*
676 *Sports Med* 2014;**2**:2325967114551328.
677 34. Chatterjee, S., Ahituv, N. Gene Regulatory Elements, Major Drivers of Human
678 Disease. *Annu Rev Genomics Hum Genet* 2017;**18**:45-63.
679 35. Dwyer, K., Agarwal, N., Pile, L. et al. Gene Architecture Facilitates Intron-Mediated
680 Enhancement of Transcription. *Front Mol Biosci* 2021;**8**:669004.
681 36. Nilsen, T.W., Graveley, B.R. Expansion of the eukaryotic proteome by alternative
682 splicing. *Nature* 2010;**463**:457-463.
683 37. Niehrs, C., Luke, B. Regulatory R-loops as facilitators of gene expression and genome
684 stability. Nature reviews *Mol Cell Biol* 2020;**21**:167-178.
685 38. Ding, F., Elowitz, M.B. Constitutive splicing and economies of scale in gene
686 expression. *Nat Struct Mol Biol* 2019;**26**:424-432.
687 39. Laxa, M. Intron-Mediated Enhancement: A Tool for Heterologous Gene Expression

For Peer Review

688 in Plants? *Front Plant Sci* 2016;**7**:1977.

689 40. Shaul, O. How introns enhance gene expression. *Int J Biochem Cell Biol* 2017;**91**:145-

690 155.

691 41. Ott, C.J., Blackledge, N.P., Kerschner, J.L. et al. Intronic enhancers coordinate

692 epithelial-specific looping of the active CFTR locus. *Proc Nat Acad Sci* 2009;**106**:19934-

693 19939.

694 42. Borsari, B., Villegas-Miron, P., Perez-Lluch, S., et al. Enhancers with tissue-specific

695 activity are enriched in intronic regions. *Genome Res* 2021;**31**:1325-1336.

696 43. Mizuhashi, K., Nagata, M., Matsushita, Y. et al. Growth Plate Borderline

697 Chondrocytes Behave as Transient Mesenchymal Precursor Cells. *J Bone Min Res*

698 2019;**34**:1387-1392.

699 44. Newton, P.T., Li, L., Zhou, B. et al. A radical switch in clonality reveals a stem cell

700 niche in the epiphyseal growth plate. *Nature* 2019;**567**:234-238.

701 45. Jacobsen, S., Sonne-Holm, S., Lund, B.et al. Pelvic orientation and assessment of hip

702 dysplasia in adults. *Acta Orthop Scand* 2004;**75**:721-729.

703 46. Jacobsen, S., Sonne-Holm, S., Soballe, K. et al. Radiographic case definitions and

704 prevalence of osteoarthrosis of the hip: a survey of 4 151 subjects in the Osteoarthritis

705 Substudy of the Copenhagen City Heart Study. *Acta Orthop Scand* 2004;**75**:713-720.

For Peer Review

47. Beck, M., Kalhor, M., Leunig, M. et al. Hip morphology influences the pattern of damage to the acetabular cartilage: femoroacetabular impingement as a cause of early osteoarthritis of the hip. *J Bone Joint Surg Br* 2005;**87**:1012-1018.

48. Ahedi, H.G., Aspden, R.M., Blizzard, L.C. et al. Hip Shape as a Predictor of Osteoarthritis Progression in a Prospective Population Cohort. *Arth Care Res* 2017;**69**:1566-1573.

49. Puliyel, J.M., Puliyel, M.M., Varughese, S. The trichorhinophalangeal syndrome with repeated dislocation of the patella. *Clin Genet* 1992;**41**:139-142.

50. Sarin, V.K., Erickson, G.M., Giori, N.J. et al. Coincident development of sesamoid bones and clues to their evolution. *Anat Rec* 1999;**257**:174-180.

51. Eyal, S., Blitz, E., Shwartz, Y. et al. On the development of the patella. *Development* 2015;**142**:1831-1839.

52. Sutton, F.S., Jr., Thompson, C.H., Lipke, J. et al. The effect of patellectomy on knee function. *J Bone Joint Surg Am* volume 1976;**58**:537-540.

53. Schindler, O.S., Scott, W.N. Basic kinematics and biomechanics of the patello-femoral joint. Part 1: The native patella. *Acta Orthop Bel* 2011;**77**:421-431.

54. Bicos, J., Carofino, B., Andersen, M. et al. Patellofemoral forces after medial patellofemoral ligament reconstruction: a biomechanical analysis. *J Knee Surg*

For Peer Review

2006;**19**:317-326.

55. McConnell, J. Rehabilitation and nonoperative treatment of patellar instability. *Sp Med Arthrosc Rev* 2007;**15**:95-104.

56. Driessen, A., Balke, M., Offerhaus, C. et al. The fabella syndrome - a rare cause of posterolateral knee pain: a review of the literature and two case reports. *BMC Muscul Dis* 2014;**15**:100.

57. Zhu, M., Metzen, F., Hopkinson, M. et al. Ablation of collagen XII disturbs joint extracellular matrix organization and causes patellar subluxation. *iScience* 2023;26:107225.

58. Buenrostro, J.D., Wu, B., Chang, H.Y. et al. ATAC-seq: A Method for Assaying Chromatin Accessibility Genome-Wide. *Cur Prot Mol Biol* 2015;**109**:21 29 21-21 29 29.

59. Gosset, M., Berenbaum, F., Thirion, S. et al. Primary culture and phenotyping of murine chondrocytes. *Nat Protoc* 2008;**3**:1253-1260.

60. Langmead, B., Salzberg, S.L. Fast gapped-read alignment with Bowtie 2. *Nat Methods* 2012;**9**:357-359.

61. Zhang, Y., Liu, T., Meyer, C.A. et al. Model-based analysis of ChIP-Seq (MACS). *Genome Biol* 2008;**9**:R137.

62. Ernst, J., Kheradpour, P., Mikkelsen, T.S. et al. Mapping and analysis of chromatin

For Peer Review

state dynamics in nine human cell types. *Nature* 2011;**473**:43-49.

63. Nakato, R., Sakata, T. Methods for ChIP-seq analysis: A practical workflow and advanced applications. *Methods* 2021;**187**:44-53.

64. Atsumi, T., Miwa, Y., Kimata, K. et al. A chondrogenic cell line derived from a differentiating culture of AT805 teratocarcinoma cells. *Cell Differ Dev* 1990;**30**:109-116.

65. Shukunami, C., Shigeno, C., Atsumi, T. et al. Chondrogenic differentiation of clonal mouse embryonic cell line ATDC5 in vitro: differentiation-dependent gene expression of parathyroid hormone (PTH)/PTH-related peptide receptor. *J Cell Biol* 1996;**133**:457-468.

66. Abe, M., Michikami, I., Fukushi, T. et al. (2010). Hand2 regulates chondrogenesis in vitro and in vivo. *Bone* 2010;**46**:1359-1368.

67. Michikami, I., Fukushi, T., Tanaka, M. et al. Kruppel-like factor 4 regulates membranous and endochondral ossification. *Exp Cell Res* 2012;**318**:311-325.

68. McLeod, M.J. Differential staining of cartilage and bone in whole mouse fetuses by alcian blue and alizarin red S. *Teratology* 1980;**22**:299-301.

69. Kuroda, Y., Rai, A., Saito, M. et al. Anatomical variation of the Psoas Valley: a scoping review. *BMC Muscul Dis* 2020;**21**:219.

70. Takeuchi, Y., Tatsuta, S., Kito, A. et al. Kruppel-like factor 4 upregulates matrix metalloproteinase 13 expression in chondrocytes via mRNA stabilization. *Cell Tissue*

For Peer Review

Res 2020;**382**:307-319.

71. Fujikawa, J., Takeuchi, Y., Kanazawa, S. et al. Kruppel-like factor 4 regulates matrix metalloproteinase and aggrecanase gene expression in chondrocytes. *Cell Tissue Res* 2017;**370**:441-449.

For Peer Review

Legends to Figures

Figure 1. Identification of putative enhancers around the *Trps1* gene.

(A) Open chromatin regions and histone modification (H3K4me2 and H3K27ac) identified by ATAC-seq and ChIP-seq in murine primary costal chondrocytes. Overhead view of the murine *Trps1* genomic region (upper image) and magnified view of the first intron (lower image). The first intron of the murine *Trps1* genomic region is highlighted by a red dotted square. Overlapping regions of ATAC-seq and ChIP-seq peaks within the first intron of *Trps1* are highlighted by a pink box. Enhancer 2 (Enh2; Chr15:50885838-50889066) and enhancer 3 (Enh3; Chr15:50868499-50872947) are labeled with red and blue bars, respectively.

(B) Genomic alignment of the *Trps1* gene loci of multiple species. Evolutionary conserved sequence alignment of multiple genomes was performed using the ECR program from Dcode.org (http://www.dcode.org).

(C) Luciferase reporter assays for Emh2 and Enh3 in chondrocytic ATDC5 cells. Enh2-, Enh3-, or Enh2-Enh3-containing pGL3-promoter luciferase vectors were transfected into chondrocytic ATDC5 cells. Cell lysate was harvested after 40 hours post-transfection for dual-luciferase assay (*$P < 0.05$).

For Peer Review

(D) Luciferase reporter assays for Enh2 deletion mutants in chondrocytic ATDC5 cells. pGL3-promoter luciferase vectors carrying deleted versions of Enh2 were transfected into ATDC5 cells. Cell lysate was harvested after 40 hours post-transfection for dual-luciferase assay (*P < 0.05).

Figure 2. *Trps1*$^{-/-}$ mice display abnormal coxal bone morphogenesis.

(A1) Expression of *Trps1* detected by *in situ* hybridization in the developing hip joint of E12.5 WT embryo. V and D indicate the ventral and dorsal sides, respectively.

(A2 and A3) Sox9 protein localization was detected by immunohistochemistry in the developing hip region of E12.5 WT (A2) and *Trps1*$^{-/-}$ (A3) embryos.

(B and C) Lateral views of the hindlimb (B) and coxal bone (C) of E15.5 WT and *Trps1*$^{-/-}$ embryos. Arrowheads in (C) indicates the mineralized region at the primary ossification center within the ilium.

(D-F) Medial views of hindlimbs (D), coxal bone (E), and pelvic bone (F) of E17.5 WT (left), *Trps1*$^{+/-}$ (mid), and *Trps1*$^{-/-}$ (right) embryos. Double arrows in (E) indicated the rostral-caudal length which is shorter in *Trps1*$^{-/-}$ embryos compared to others. Arrowheads in (E) indicate the reduced range of the mineralized region within the primary ossification center of the ischium and pubis in *Trps1*$^{-/-}$ embryos. In (F), the angle between the ilium and pubis was highlighted. (G)

For Peer Review

The measurements of the ilio-pubic angle show that the angle is smaller in *Trps1*$^{-/-}$ embryos than others (n=3 used for each genotype).

Key; ac: primordium of acetabulum, co: primordium of os coxa, fe: femur, fi: fibula. hg: hindgut. il: ilium, is: ischium, pu: pubis, ti: tibia.

Figure 3. Delayed maturation of the ilio-pubic junction and abnormal psoas valley invagination in *Trps1*$^{\Delta int/\Delta int}$ mice.

(A-D) Ventral view of 3D-CT (A and B) and toluidine blue-stained frontal section (C and D) of the hip joint in the 1-month-old control and *Trps1*$^{\Delta int/\Delta int}$ mice. Arrowheads in (B) indicate the mildly expanded width between the mineralized ilium and pubis in *Trps1*$^{Dint/Dint}$ mice. Double arrows in (C) and (D) indicate the cartilaginous region at the ilio-pubic junction.

(E-H) HE-stained frontal sections (E and F) and ventral views of reconstructed 3D-CT (G and H) of the hip joint in the 3-month-old control and *Trps1* $^{\Delta int/\Delta int}$ mice. The arrowhead in (H) points to the deeply invaginated psoas valley in *Trps1*$^{Dint/Dint}$ mice.

(I and J) Measurement of the psoas valley depth. The measured length is indicated by the double arrow in (I). The data of the 2- to 3-month-old control (n=10) and *Trps1* $^{\Delta int/\Delta int}$ (n=12) mice are shown in (J).

For Peer Review

(K and L) Toluidine blue-stained sections of distal femur of postnatal 10-day-old control (K) and *Trps1* $^{\Delta int/\Delta int}$ (L) mice. The invaginating vascular canals into the initial developing site of the secondary ossification center (SOC) are indicated by arrows. Arrowheads in (K) indicate red blood cells (RBCs) at the central region of the distal epiphysis, while RBCs are rarely observed in the similar femoral domain of *Trps1* $^{\Delta int/\Delta int}$ pups.

(M-T) The distal femoral SOC in the 1-month-old control (M-P) or *Trps1* $^{\Delta int/\Delta int}$ (Q-T) mice. Sections stained with toluidine blue (M, M', Q, and Q') or mRNA detected by *in situ* hybridization for *Col1a1* (N and R), *Col2a1* (O and S), and *Col10a1* (P and T) are shown. Red arrowheads in (Q') and (S) indicate the remaining cartilage tissue and chondrocytes left behind at the developing SOC.

Key; fh: femoral head, il: ilium, isc: ischium, pu: pubis.

Figure 4. Skeletal defects in 3-month-old *Trps1*$^{\Delta int/-}$ mice.

(A and B) Ventral views of the dissected anatomy of the hip joint region in the control (A) and *Trps1*$^{\Delta int/-}$ (B) mice. Red dashed lines indicate the acetabular rim, which shows smooth parabolic shape and wedged-shape in the control and *Trps1*$^{\Delta int/-}$ mice, respectively.

For Peer Review

(C and D) Ventral views of reconstructed 3D-CT of hip joint in the control (C) and *Trps1*$^{\Delta int/-}$ (D) mice. Arrowheads highlight deeply invaginated psoas valley, resulting in severe under-coverage of the femoral head within the acetabulum in *Trps1*$^{\Delta int/-}$ mice (D).

(E-H) Transverse sections of the hip joint stained with HE (E and F) and toluidine blue (G and H) in the control (E and G) and *Trps1*$^{\Delta int/-}$ (F and H) mice. (G) and (H) show magnified views of areas surrounded by squares in (E) and (F), respectively, on serial sections. Arrowheads in (H) point to the toluidine blue-positive remaining cartilaginous tissue at the ilio-pubic junction in *Trps1*$^{\Delta int/-}$ mice.

(I-L) Frontal (I and J) and medial (K and L) views of reconstructed 3D-CT of knee joints in the control (I and K) and *Trps1*$^{\Delta int/-}$ (J and L) mice. Medially dislocated patella in *Trps1*$^{\Delta int/-}$ mice is labelled as pt* in (J) and (L). The arrowheads in (J) points to the flattened trochlear groove in *Trps1*$^{Dint/-}$ mice. Arrowheads in (K) and (L) point to the fabella formed within the lateral head of the gastrocnemius muscle. Red dashed lines indicate a round parabolic and straightly shaped surface of the distal femur in the control (K) and *Trps1*$^{\Delta int/-}$ mice (L), respectively. See also (M) and (N).

(M and N) Tomography images at the sagittal mid-planes of the distal femurs in control (M) and *Trps1*$^{\Delta int/-}$ (N) mice. Red dashed lines indicate articular surface of the distal femur in the control (M) and *Trps1*$^{\Delta int/-}$ (N) mice. Epiphyseal bone marrow space is labelled with yellow asterisks.

For Peer Review

(O) Ventral views of the 2-day-old knees in the control (left) and *Trps1*$^{\Delta int/-}$ (right) mice. White arrowheads in point to the stained patella.

(P-S) Low (P and Q) and high (R and S) magnified sagittal images of the distal femurs in the control (P and R) and *Trps1*$^{\Delta int/-}$ (Q and S) mice. Sections were stained with toluidine blue. Double arrows in (R) and (S) indicate epiphyseal growth plate chondrocytes. The asterisk in (S) indicate abnormal accumulation of the toluidine blue-positive cartilage tissue.

Key; co: os coxa, fh: femoral head, fi; fibula, poc: primary ossification center, pt: patella, pt*; dislocated patella, soc: secondary ossification center, ti: tibia.

For Peer Review

Strain	gRNA1	gRNA2
ΔEnh1	TCCACTCCTCCCCGTTGCAAagg	GGTTAATACATGCTGGTCTTtgg
ΔEnh2	CGCTGCTGCAAGTTTTCTGGggg	ACGGGGAGCAGACTAGGCACcgg
ΔEnh3	CAGGCAAGATCAGTTCCCAAggg	ACTTTAGGAACAAAACACCagg
ΔEnh2/3 (Δint)	CGCTGCTGCAAGTTTTCTGGggg	CAGGCAAGATCAGTTCCCAAggg

Table 1. Sequences of guide RNAs used in this study

allele	Forward primer	Reverse primer
Trps1 mut	CCACACACTATTTTCCATGGG	CCCCTTCTATCGCCTTCTTGA
Trps1 wt	TAGTAAAGCAGGCCGTGAAG	ACCCAAAGGTCACTTACTGG
Enh1 mut	TTGCCTGATACTGCAGAGT	TGAGGTTGATATGGTTTTCTG
Enh1 wt	AATCAGTGAAAAATATTTGAG	TGAGGTTGATATGGTTTTCTG
Enh2 mut	GCAAGCTCATACAACTTGCCTGT	ACTCCCCCAATTCCTCTTTTCTC
Enh2 wt	GACGGGTATACCAGGAGAGGATG	ACTCCCCCAATTCCTCTTTTCTC
Enh3 mut	TAGTCAAGTCCACAGGTGGGAAA	AGGACTTCCACTTTACGGAAGC
Enh3 wt	TAGTCAAGTCCACAGGTGGGAAA	ATAGAACAAGTGGCTCCCAGCTC
Enh2/3 mut (Δint mut)	TAGTCAAGTCCACAGGTGGGA AA	ACTCCCCCAATTCCTCTTTTCTC
Enh2/3 wt (Δint wt)	GAAAATGGACCCTGAGGCTTATG	AAAATGCAAGCTTGGTTTGGTTT

Table 2. List of genotyping primers used in this study

For Peer Review

Deletion of Trps1 regulatory elements recapitulates postnatal hip joint abnormalities and growth retardation of Trichorhinophalangeal syndrome in mice

Naoya Saeki[1,2], Chizuko Inui-Yamamoto[1], Yuki Ikeda[1] , Rinna Kanai[1,3], Kenji Hata[4], Shousaku Itoh[5], Toshihiro Inubushi[6], Shigehisa Akiyama[2], Shinsuke Ohba[1,*], Makoto Abe[1,*]

[1]Department of Tissue and Developmental Biology, Osaka University Graduate School of Dentistry, Yamada-oka 1-8, Suita, Osaka 565-0871, Japan

[2]Department of Special Needs Dentistry, Osaka University Graduate School of Dentistry, Yamada-oka 1-8, Suita, Osaka 565-0871, Japan

[3]Department of Fixed Prosthodontics and Orofacial Function, Osaka University Graduate School of Dentistry, Yamada-oka 1-8, Suita, Osaka 565-0871, Japan

[4]Department of Molecular and Cellular Biochemistry, Osaka University Graduate School of Dentistry, Yamada-oka 1-8, Suita, Osaka 565-0871, Japan

[5]Department of Restorative Dentistry and Endodontology, Osaka University Graduate School of Dentistry, Yamada-oka 1-8, Suita, Osaka 565-0871, Japan

[6]Department of Orthodontics and Dentofacial Orthopedics, Osaka University

For Peer Review

Graduate School of Dentistry, Yamada-oka 1-8, Suita, Osaka 565-0871, Japan

* Corresponding author: Makoto Abe, Department of Tissue and Developmental Biology, Osaka University Graduate School of Dentistry, 1-8 Yamada-oka, Suita, Osaka 565-0871, Japan, Tel: +81-6-6879-2874, FAX: +81-6-6879-2875, Email: makoto.abe.dent@osaka-u.ac.jp

* Corresponding author: Shinsuke Ohba, Department of Tissue and Developmental Biology, Osaka University Graduate School of Dentistry, 1-8 Yamada-oka, Suita, Osaka 565-0871, Japan, Tel: +81-6-6879-2871, FAX: +81-6-6879-2875, Email: ohba.shinsuke.dent@osaka-u.ac.jp

For Peer Review

Abstract

Trichorhinophalangeal syndrome (TRPS) is a genetic disorder caused by point mutations or deletions in the gene-encoding transcription factor TRPS1. TRPS patients display a range of skeletal dysplasias, including reduced jaw size, short stature, and a cone-shaped digit epiphysis. Certain TRPS patients experience early onset coxarthrosis that leads to a devastating drop in their daily activities. The etiologies of congenital skeletal abnormalities of TRPS were revealed through the analysis of *Trps1* mutant mouse strains. However, early postnatal lethality in *Trps1* knockout mice has hampered the study of postnatal TRPS pathology. Here, through epigenomic analysis we identified two previously uncharacterized candidate gene regulatory regions in the first intron of *Trps1*. We deleted these regions, either individually or simultaneously, and examined their effects on skeletal morphogenesis. Animals that were deleted individually for either region displayed only modest phenotypes. In contrast, the *Trps1*$^{\Delta int/\Delta int}$ mouse strain with simultaneous deletion of both genomic regions exhibit postnatal growth retardation. This strain displayed delayed secondary ossification center formation in the long bones and misshaped hip joint development that resulted in acetabular dysplasia. Reducing one allele of the *Trps1* gene in *Trps1*$^{\Delta int}$ mice resulted in medial patellar dislocation that has been observed in some patients with TRPS. Our novel *Trps1* hypomorphic strain

For Peer Review

recapitulates many postnatal pathologies observed in human TRPS patients, thus positioning this strain as a useful animal model to study postnatal TRPS pathogenesis. Our observations also suggest that *Trps1* gene expression is regulated through several regulatory elements, thus guaranteeing robust expression maintenance in skeletal cells.

For Peer Review

Introduction

Trichorhinophalangeal syndrome (TRPS) is an autosomal-dominant genetic disorder caused by mutations or deletions in the transcription factor TRPS1 [1]. The occurrence rate of TRPS is extremely low and is estimated to be 1 in 50,000 live births [2]. Patients with TRPS display several congenital skeletal pathologies, including micrognathia, a cone-shaped epiphysis of the phalangeal bone, short stature, and hip joint dysplasia (OMIM #150230, #190350, #190351). Growth failure becomes pronounced as patients grow, and many patients suffer from early onset coxarthritis [3]. The role of TRPS1 during embryonic long bone development has been thoroughly investigated using murine models of TRPS [4-8]. The lack of *Trps1* in mice results in reduced chondrocyte proliferation and delayed hypertrophic differentiation of long bone epiphyseal and temporomandibular joint growth plates [5; 8]. These changes involve altered Wnt5a-, Pthlh-, Hedgehog-, and Stat3-mediated signaling due to the absence of *Trps1* [8-12]. In addition, altered growth plate characteristics indirectly lead to the uncoupling of growth plate maturation rate and perichondrial ossification in *Trps1* mutant mice, ultimately resulting in accelerated bone collar formation [6]. These observations underscore the crucial role of Trps1 during endochondral ossification of long bone.

Despite accumulating knowledge regarding TRPS1 during embryonic long bone

For Peer Review

development, the etiologies of postnatal skeletal pathologies of TRPS remain elusive [2]. Greater than 50% of patients with TRPS experience developmental dysplasia of the hip [2; 3; 13]. The femoral heads of young patients with TRPS display Perthes disease-like symptoms, although the damaged joints do not recover [14-18]. This clinical evidence indicates the crucial role(s) played by TRPS1 in the context of joint development and postnatal maintenance at various anatomical sites; however, few studies have described the exact roles played by Trps1 in hip joint development.

The hind limbs of tetrapods are derived from the pelvic fins of ancestral fishes [19]. Although the pelvic fins in fish are considered to play minor roles in swimming, they have clearly shifted to robust weight-bearing limbs in tetrapods [20]. The pelvic girdle connects the axial and hindlimb skeletons. Unlike the long bones, os coxae (hip bones) form through the gradual fusion of three initially separated bones, including the ilium, ischium, and pubis. Each bone piece is formed through endochondral ossification that is initiated by the condensation of mesenchymal cells originating from the mesodermal cells of the somatopleure [21]. The cartilage primordium of the ilium, ischium, and pubis fuses and establishes a complex triradiate zone at the site of the future acetabulum, where the femoral heads articulate. In humans, primary ossification centers are sequentially formed, first in the ilium primordium and then in the ischium and pubis

For Peer Review

[22]. Secondary ossification occurs at multiple locations in the pelvis that include the iliac crest, the pubic symphysis, and the ischial tuberosity [23]. The triradiate zone of the acetabulum remains un-ossified until mid-puberty and functions as a cartilaginous growth plate that allows the acetabulum to expand to accommodate the enlarging femoral head [24].

As the pelvis is one of the weight-bearing joints in all terrestrial animals, precise morphogenesis of the hip joint structure is crucial for locomotion. Indeed, the hip joint morphology appears quite delicate, and both under- and over-coverage of the acetabulum on the femur raises clinical issues such as acetabular dysplasia or femoroacetabular impingement (FAI) [25-27]. Severe under-coverage can cause hip instability, subluxation, or dislocation [28; 29]. Increased stress due to under-coverage is one of the causes of acetabular labral hypertrophy and tears that, in some cases, force joint surgery to prevent the onset of coxarthritis [30].

In this report, we describe developmental dysplasia of the hip during the embryonic stages in newly developed *Trps1* hypomorphic mouse strains. *Trps1* hypomorphic mice survived postnatally but displayed under-coverage of the femoral head in the acetabulum. Further reduction in *Trps1* gene dosage resulted in a reduced survival rate; however, surviving adult mice exhibited major skeletal abnormalities observed in human

For Peer Review

TRPS patients. These observations reinforce the crucial roles played by Trps1 in normal hip joint morphogenesis and partially explain the etiology of coxarthrosis observed in certain patients with TRPS.

For Peer Review

Results

1. Identification of putative enhancers in the first intron of the murine *Trps1* gene

Our previous study indicated that several *Trps1* regulatory sequence for its tissue-specific expression locates at the proximal promoter region of the *Trps1* gene [31]. As regulations of the *Trps1* gene transcription in several tissues were unclear from the previous study (e.g., growth plate chondrocytes and kidney ureteric bud), we aimed to identify other *Trps1* enhancers by uncovering the chromatin profiles at the *Trps1* gene locus in murine costal chondrocytes. Chondrocytes were used in this study, as *Trps1*$^{-/-}$ mice exhibit severe cartilage defects during the late embryonic stages [4; 6; 8; 10], and short stature is a prominent feature of postnatal human TRPS pathologies [2]. Chromatin accessibility (ATAC-seq) and histone modifications for active enhancer signatures (ChIP-seq for H3K27ac and H3K4me2) were assessed. Comparison of ATAC-seq and ChIP-seq peaks revealed that several open chromatin regions were accompanied with the active enhancer signatures (Fig. 1A). Among them, we found two prominent regions in the first intron of the *Trps1* gene body, each of which were approximately 3 kb (Enh2; Chr15:50885838-50889066) to 5 kb (Enh3; Chr15:50868499-50872947) in length (Fig. 1A). The identified mouse genomic sequence showed almost 75% homologies to human

For Peer Review

TRPS1 genomic sequences (Enh2, human Chr8:115664810-115668001; Enh3, human Chr8:115646975-115650605). Multispecies sequence alignment of the *Trps1* gene using the Evolutionary Conserved Regions (ECR) program Dcode.org (http://www.dcode.org) revealed that several intronic regions including Enh2 and Enh3, as well as the TSS proximal promoter region, were conserved between mice, humans, opossums, and chickens, while all exons displayed the highest conservation (Fig. 1B). Although frogs exhibited some alignment with other higher vertebrates within the fourth intron, similarities within the first intron were limited.

The Enh2 and Enh3 elements were cloned and inserted into a luciferase vector containing the minimum promoter. We performed luciferase assays using the vectors in ATDC5 chondrocytic cells to ask whether the two elements could induce transcriptional activation either individually or simultaneously (Fig. 1C). Enh2 augmented transcriptional activity, whereas Enh3 fragment did not (Fig. 1C). Furthermore, tandem constructs carrying both Enh2 and Enh3 induced less activities than those carrying Enh2 alone (Fig. 1C). To identify the responsible domain for transcriptional activation in Enh2, we analyzed luciferase activities using Enh2 deletion mutant constructs (each fragment of almost 1 kb in length). This assay revealed that two thirds in the 5' side of the Enh2 contains responsible elements for its activity (Fig. 1D).

For Peer Review

2. Individual deletion of Enh1, Enh2, and Enh3 causes mildly abnormal acetabular rim morphology when combined with heterozygous deletion of the *Trps1* gene

To investigate the potential *in vivo* roles of Enh2 and Enh3, we generated *Trps1*$^{\Delta Enh2/\Delta Enh2}$ and *Trps1*$^{\Delta Enh3/\Delta Enh3}$ mice, which lack Enh2 and Enh3 (Suppl. Fig. 1) using CRISPR/Cas9 genome editing. In addition to *Trps1*$^{\Delta Enh2/\Delta Enh2}$ and *Trps1*$^{\Delta Enh3/\Delta Enh3}$ mice, we also generated a mouse strain which lacks the majority of the previously identified proximal promoter sequences of *Trps1* gene (Enh1) while retaining the potential basal promoter sequence (*Trps1*$^{\Delta Enh1/\Delta Enh1}$; Suppl. Fig. 1) [31].

Trps1$^{\Delta Enh1/\Delta Enh1}$ mice were viable and gained body weight, and this did not differ from control (WT and *Trps1*$^{\Delta Enh1/+}$) mice (Suppl. Fig. 2A). *Trps1*$^{\Delta Enh2/\Delta Enh2}$ (Suppl. Fig. 2B) and *Trps1*$^{\Delta Enh3/\Delta Enh3}$ (Suppl. Fig. 2C) mice were also viable and gained body weight compared to their control mice. The genotype distribution at the weaning time were as predicted in all three strains, thus indicating that the Enh1 (Suppl. Fig. 2D), Enh2 (Suppl. Fig. 2E), and Enh3 (Suppl. Fig. 2F) sequence deletion did not affect the survival rate during this developmental period. As *Trps1* conventional knockout mice display numerous skeletal abnormalities at the embryonic stage, we analyzed *Trps1*$^{\Delta Enh1/\Delta Enh1}$, *Trps1*$^{\Delta Enh2/\Delta Enh2}$, and *Trps1*$^{\Delta Enh3/\Delta Enh3}$ neonates (PNd0; Suppl. Figs. 2G-2R). The

For Peer Review

morphology and sizes of the craniofacial (Suppl. Figs. 2G, 2J, 2M, and 2P), the forelimb skeletons (Suppl. Figs. 2H, 2K, 2N, and 2Q), and hindlimb (Suppl. Figs 2I, 2L, 2O, and 2R) appeared normal in *Trps1*$^{\Delta Enh1/\Delta Enh1}$ (Suppl. Figs. 2J-2L), *Trps1*$^{\Delta Enh2/\Delta Enh2}$ (Suppl. Figs. 2M-2O), and *Trps1*$^{\Delta Enh3/\Delta Enh3}$ (Suppl. Figs. 2P-2R) mice compared to the WT control mice (Suppl. Figs. 2G-2I).

The skeletal morphology of *Trps1*$^{\Delta Enh1/\Delta Enh1}$ (Suppl. Figs. 3C, 3K, and data not shown), *Trps1*$^{\Delta Enh2/\Delta Enh2}$ (Suppl. Figs. 3E, 3M, and data not shown), and *Trps1*$^{\Delta Enh3/\Delta Enh3}$ (Suppl. Figs. 3G, 3O, and data not shown) at the postnatal mature stage was overtly normal in 3D-CT images compared to the wild-type (Suppl. Figs. 3A, 3I, and data not shown) or *Trps1*$^{+/-}$ mice (Suppl. Figs. 3B, 3J, and data not shown). However, simultaneous deletion of Enh1 and another allele of *Trps1* gene (*Trps1*$^{\Delta Enh1/-}$), which was assumed to result in reduced baseline *Trps1* expression compared to homozygous deletion of Enh1 (*Trps1*$^{\Delta Enh1/\Delta Enh1}$), resulted in deeper invagination of the psoas valley of the hip joint than the other control mice (Suppl. Fig. 3D). The knee joints of *Trps1*$^{\Delta Enh1/-}$ mice appeared normal in both 3D-CT images and histological sections (Suppl. Figs. 3L and data not shown). *Trps1*$^{\Delta Enh2/-}$ (Suppl. Fig. 3F) and *Trps1*$^{\Delta Enh3/-}$ (Suppl. Fig. 3H) mice, which one allele of the *Trps1* gene was deleted, also showed modestly deepened psoas valley, which resulted in a small under-coverage of the femoral head by the acetabulum. Knee joints

For Peer Review

of *Trps1*$^{\Delta Enh2/-}$ (Suppl. Figs. 3N and data not shown) and *Trps1*$^{\Delta Enh2/-}$ (Suppl. Fig. 3P and data not shown) mice appeared normal in both 3D-CT images and histological sections. Thus, individual deletions of Enh1, Enh2, or Enh3 only result in modest skeletal phenotypes in mice.

3. *Trps1*$^{-/-}$ mouse embryos show defects in pelvic bone ossification

We observed modest hip joint abnormalities in *Trps1*$^{\Delta Enh1/-}$, *Trps1*$^{\Delta Enh2/-}$, *Trps1*$^{\Delta Enh3/}$ mice. It has been established that a high proportion of patients with TRPS experience early onset coxarthritis [2]. Although *Trps1*$^{-/-}$ mice have been used to investigate the skeletal pathologies of TRPS, hip joint formation in this mutant strain has not yet been examined in detail. Therefore, we set out to address this issue in *Trps1*$^{-/-}$ mice (Fig. 2). *Trps1* was expressed in the hip joint region between the developing acetabulum of the coxa and the femoral head at E12.5 (Fig. 2A1). The cartilage primordia of both coxa and femur, which were characterized by Sox9 expression, were normally formed in WT (Fig. 2A2) and *Trps1*$^{-/-}$ (Fig. 2A3) embryos. At E15.5, the pelvic bone (os coxa), femur, tibia, and fibula containing mineralized primary ossification centers were observed in WT, *Trps1*$^{+/-}$, and *Trps1*$^{-/-}$ embryos (Figs. 2B and 2C, and data not shown). Although pelvic bone exhibited ossification in the iliac portion and length of pelvis was similar in WT and *Trps1*$^{-/-}$

For Peer Review

embryos, mineralized region was limited in *Trps1*$^{-/-}$ embryos (arrowheads in Fig. 2C). At E17.5, although primary ossification of the ilium, ischium, and pubis was initiated in WT, *Trps1*$^{+/-}$, and *Trps1*$^{-/-}$ embryos, the length of pelvic bone was shorter in *Trps1*$^{-/-}$ embryos (Figs. 2D, 2E). Furthermore, the lateral view of the pelvic bone revealed that the angle between the anterior (ilium) and posterior (ischium and pubis) portion is sharply bent in *Trps1*$^{-/-}$ embryos compared to WT and *Trps1*$^{+/-}$ (Fig. 2F, 2G). Thus, the global lack of *Trps1* results in developmental abnormalities in mineralization, growth, and morphological curvature of the coxa.

3. *Trps1*$^{\Delta int/\Delta int}$ mice lacking both Enh2 and Enh3 displayed growth delays and skeletal defects

To examine the potential cooperative effects of Enh2 and Enh3 on *Trps1* expression and skeletal development, we generated mutant mice lacking a 20 kb region within the first intron of *Trps1*, which contains both Enh2 and Enh3, by genome editing (Suppl. Fig. 1). Homozygous intron knockout mice (referred to as *Trps1*$^{\Delta int/\Delta int}$ mice hereafter) survived postnatally and were fertile, even in *Trps1*$^{\Delta int/\Delta int}$ male and female mating pairs. The number of *Trps1*$^{\Delta int/\Delta int}$ mice at postnatal 3 weeks was slightly lower than expected, thus suggesting that some *Trps1*$^{\Delta int/\Delta int}$ mice died before weaning (Suppl. Fig. 4A). *Trps1*$^{\Delta int/\Delta int}$

For Peer Review

mice exhibited significantly lower body weight during postnatal periods (statistically significant through postnatal weeks 3 to 9) compared to that of the WT or *Trps1*$^{\Delta int/+}$ mice (Suppl. Fig. 4B). When expression level of *Trps1* was examined in several organs of the early postnatal pups (Suppl. Fig. 4C), *Trps1* levels were significantly reduced in the kidney, pelvis, scapula, and rib cartilage of *Trps1*$^{\Delta int/\Delta int}$ mice (Suppl. Fig. 4C). The reduction in *Trps1* expression was mild in the pelvic and rib cartilage. In contrast, there were no significant changes in *Trps1* expression in the heart or skin, and vibrissa follicle of *Trps1*$^{\Delta int/\Delta int}$ mice. *Trps1* expression was also assessed in cultured costal chondrocytes prepared from the WT, *Trps1*$^{\Delta Enh2/\Delta Enh2}$, *Trps1*$^{\Delta Enh3/\Delta Enh3}$, and *Trps1*$^{\Delta int/\Delta int}$ mice (Suppl. Fig. 4D). In *Trps1*$^{\Delta int/\Delta int}$ chondrocytes, the *Trps1* expression level was significantly decreased to approximately 40% of the WT; the level was also significantly reduced in *Trps1*$^{\Delta Enh3/\Delta Enh3}$ chondrocytes (Suppl. Fig. 3D), whereas the reduction was mild compared to that in the cells of *Trps1*$^{\Delta int/\Delta int}$ pups.

We next analyzed the skeletons of newborn *Trps1*$^{\Delta int/\Delta int}$ pups (Suppl. Figs. 4). Compared to the control pups, *Trps1*$^{\Delta int/\Delta int}$ pups showed no obvious defects in their body size (Suppl. Fig. 5A). The morphologies of the head and neck skeletons (Suppl. Figs. 5B-5G), the mineralization of the vertebral body and arches (Suppl. Figs. 5H-5M), the morphogenesis and ossification of the forelimb morphogenesis and ossification were

For Peer Review

normal in these mutants (Suppl. Figs. 5N-5Q), the gross appearance of the hind limb was also similar between the control and mutants (Suppl. Figs. 5R-5U). However, *Trps1*$^{\Delta int/\Delta int}$ pups displayed 14% reduction in the size of the pelvis (Suppl. Fig. 5T; P<0.001) and a tendency of reduction in the length of the femur (Fig. 5U).

4. Adult *Trps1*$^{\Delta int/\Delta int}$ mice display developmental delays in formation of pelvic girdle and secondary ossification center

The defects of the pelvis and femur in *Trps1*$^{\Delta int/\Delta int}$ mice led us to focus on their hip joints. They survived to the mature stage, and this allowed us to examine the postnatal structure of the hip joint in these mutants. At 1-month postnatal, 3D-CT images showed well-mineralized hip bones in both control (Fig. 3A) and *Trps1*$^{\Delta int/\Delta int}$ mice (Fig. 3B). The cartilaginous ilio-pubic junction appeared to be wider in *Trps1*$^{\Delta int/\Delta int}$ mutants at this developmental stage (arrowheads in Fig. 3B). Histological analysis revealed that the cartilaginous remnants between the ilio-pubic junctions were more abundant in *Trps1*$^{\Delta int/\Delta int}$ mice (Fig. 3D), whereas they were in the well-defined narrow cartilaginous domains in the control mice (Fig. 3C). At 3-months postnatal, the cartilaginous ilio-pubic junctional domain were replaced by mature bone in both control (Fig. 3E) and *Trps1*$^{\Delta int/\Delta int}$ mice (Fig. 3F). However, 3D-CT images showed that the psoas valley of

For Peer Review

Trps1$^{\Delta int/\Delta int}$ mice (arrowheads in Fig. 3H) was more deeply invaginated than that of control mice (Fig. 3G), thus resulting in increased psoas valley depth in the mutants (Figs. 3I and 3J).

The formation of a secondary ossification center (SOC) is crucial for reducing the physical impact of the cartilaginous epiphyseal growth plate [32]. On day 10 postnatal, in *Trps1*$^{\Delta int/\Delta int}$ mice (Fig. 3L) the initiation of SOC formation was delayed compared to that in control mice (Fig. 3K); both vascular canal invasion and hypertrophic differentiation of the epiphyseal resting chondrocytes were delayed in *Trps1*$^{\Delta int/\Delta int}$ mice. In the first postnatal month when the SOC is usually fully formed, the SOC was formed in both the control (Figs. 3M and 3M') and the *Trps1*$^{\Delta int/\Delta int}$ mice (Figs. 3Q and 3Q'). Osteoblasts expressing *Col1a1* were observed in the SOC of the control (Fig. 3N) and *Trps1*$^{\Delta int/\Delta int}$ mice (Fig. 3R). However, cartilaginous remnants stained for toluidine blue (see red arrowheads in Fig. 3Q' compared to Fig. 3M') were detected in the *Trps1*$^{\Delta int/\Delta int}$ SOC; cells in the remnants expressed *Col2a1* (see red arrows in Fig. 3S compared to Fig. 3O) but not *Col10a1* (Figs. 3P and 3T). Thus, adult *Trps1*$^{\Delta int/\Delta int}$ mice exhibited developmental delays in coxa and SOC formation. Furthermore, *Trps1*$^{\Delta int/\Delta int}$ mice displayed an increase in the psoas valley depth, possibly resulting in regional under-coverage of the femoral head within the acetabulum.

For Peer Review

5. *Trps1*$^{\Delta int/-}$ mice display reduced survival rates, severe growth defects, acetabular dysplasia, and patella dislocation.

Trps1$^{\Delta int/-}$ mice were generated by mating *Trps1*$^{\Delta int}$ mice with *Trps1*$^{+/-}$ mice. Timed mating embryos were collected at E17.5. *Trps1*$^{\Delta int/-}$ embryos were visually indistinguishable from WT embryos (Suppl. Fig. 6A). However, on postnatal day 5 (Suppl. Fig. 6B) or at later mature stages (Suppl. Fig. 6C), *Trps1*$^{\Delta int/-}$ mice were significantly smaller. Also, the number of the *Trps1*$^{\Delta int/-}$ animals surviving to the weanling stage were extremely low compared to other genotypes (Suppl. Fig. 6D).

We first analyzed skeletal development of *Trps1*$^{\Delta int/-}$ embryos at E18.5 (Suppl. Figs. 6E-6Q). As described above, body size was comparable between control and *Trps1*$^{\Delta int/-}$ embryos (Suppl. Fig. 6E). Control and *Trps1*$^{\Delta int/-}$ embryos demonstrated no obvious difference in craniofacial skeletons (Suppl. Figs. 6F-6I, 6L, and 6M), appendicular skeletons (Suppl. Figs. 6J, 6K), sternum (Suppl. Figs. 6N and 6O), and rib cage (Suppl. Figs. 6P and 6Q). Thus, despite the postnatal growth defects of *Trps1*$^{\Delta int/-}$ mice, their embryonic skeletal defects were negligible small.

We analyzed *Trps1* expression in tissues harvested from rib, knee, vertebral cartilage and kidney from postnatal day 0 pups (Suppl. Figs. 7A-7D). The expression level of *Trps1*

For Peer Review

showed increased tendency in *Trps1*$^{+/-}$ mice, while *Trps1* expression was not significantly reduced in *Trps1*$^{\Delta int1/-}$ tissues obtained from rib (Suppl. Fig. 7A), knee (Suppl. Fig. 7B), and vertebral cartilage (Suppl. Fig. 7C). In contrast, *Trps1* expression in *Trps1*$^{\Delta int/-}$ neonate kidney showed significant reduction (Suppl. Fig. 7D).

We obtained two surviving *Trps1*$^{\Delta int/-}$ mice at the weaning stage (Suppl. Fig. 6D). These mice survived for more than 3 months postnatally (samples were collected at 3- and 6-months postnatally). They were both female, but neither gave birth to pups. Macroscopic anatomy (Figs. 4A and 4B) and 3D-CT analysis (Figs. 4C and 4D) revealed a deeply invaginated psoas valley together with severe under-coverage of the femoral head within the acetabulum. Histologically, the cartilaginous ilio-pubic junction remained even in 3-month-old *Trps1*$^{\Delta int/-}$ mice (Figs. 4F and 4H), but not in the control mice (Figs. 4E and 4G).

3D-CT analysis also revealed other skeletal pathologies of the *Trps1*$^{\Delta int/-}$ mice, including the medial dislocation of the patella (Figs. 4I and 4J; observed in four out of four knees), reduced development of the fabella that is a sesamoid bone embedded in the lateral head of the gastrocnemius muscle (Figs.4K and 4L; observed in four out of four knees), shallow and flattened trochlear groove (Figs. 4J and 4L; observed in four out of four knees), and reduced area of the SOC domain (Figs. 4M and 4N). Given that the patellar dislocation

For Peer Review

was not observed in perinatal *Trps1*$^{\Delta int/-}$ pups (Fig.4O), dislocation was likely to occur postnatally in the mutants. Histologically, *Trps1*$^{\Delta int/-}$ mice showed not just the reduced size of the SOC, but also the presence of cartilaginous remnant even at 3-months postnatal (Figs. 4P-4S). Thus, *Trps1*$^{\Delta int/-}$ mice displayed more severe pathologies than *Trps1*$^{\Delta int/\Delta int}$ mice.

For Peer Review

Discussion

The pelvic girdle functions as a load-bearing structure in both bipedal and quadrupedal animals. The precise morphogenesis and alignment of the pelvis, femur, and other joint structures are crucial for tolerating various types and times of hip joint movement without friction. Compared to the knowledge of genes involved in fore- and hindlimb development, much less is known regarding the genetic regulation of pelvic girdle development. Here, we demonstrate that the transcription factor Trps1 is important for normal pelvic development. We observed that the size relationship between the femoral head and acetabulum was altered when the expression of *Trps1* was low. In particular, the development of the pubic bone was mostly affected, and the acetabulum of the ilio-pubic junction exhibited under-coverage of the femoral head. These observations reinforce the indispensable role of Trps1 in the normal pelvic girdle morphogenesis. The psoas valley is an anterior depression located at the acetabular rim and coincides with a site commonly associated with acetabular labral pathology [33]. The invagination of the psoas valley was severely affected in $Trps1^{\Delta int/\Delta int}$ and surviving $Trps1^{\Delta int/-}$ mice. This phenotype may partly explain the etiology of frequently observed hip dysplasia and early onset coxarthrosis in patients with TRPS.

For Peer Review

1. Postnatal skeletal dysplasia by deletion of potential regulatory elements in the first intron of murine *Trps1* gene

Our understanding of the transcriptional regulation of *Trps1* expression is still limited. Advances in high-throughput sequencing have revealed chromatin accessibility, chromatin modifications, and transcription factor binding sites [34]. The functional significance of computational data from ATAC-seq and ChIP-seq needs to be verified experimentally, most ideally by *in vivo* strategies. We identified several enhancer candidates in the murine *Trps1* gene region that were mostly regionalized to the 5' side of the first intron. This genomic region is well conserved in mammals (opossums and humans), whereas the chicken sequence is much less conserved. To examine their biological significance, we deleted the identified sequences using genome editing approaches in mice. Furthermore, we generated compound heterozygous mice in which the enhancers were deleted with a disrupted *Trps1* gene in another allele.

Chondrocytes derived from $Trps1^{\Delta int/\Delta int}$ mice exhibited an approximately 60% reduction in *Trps1* expression compared to the WT cells. Interestingly, chondrocytes harvested from $Trps1^{\Delta Enh3/\Delta Enh3}$ mice also exhibited reduced *Trps1* expression (and $Trps1^{\Delta Enh2/\Delta Enh2}$ exhibited a tendency for reduction) compared to the WT cells. This observation indicated that there were at least two independent enhancers, which regulates *Trps1* expression,

For Peer Review

within the first intron of the *Trps1* gene.

The presence of introns in the gene body is known to play various roles in the cell, where 1) they upregulate transcription through intron-mediated enhancement of transcription [35], 2) they increase proteomic complexity through alternative splicing [36], and 3) they alleviate the genotoxic R-loop formation that appears during the transcriptional process [37]. Introns can regulate gene expression, where they reside both at the level of transcription [38] and post-transcriptionally [39; 40]. Recent evidence suggests that many key cis-regulatory regions are located in the introns of their target genes [41]; especially, tissue-specific enhancers are highly enriched in intronic regions, regulating the expression of genes that function in tissue-specific manners [42]. Furthermore, an intergenic-to-intronic active enhancer continuum is observed during the transition from developmental to adult stages; the most differentiated tissues tend to exhibit higher rates of intronic enhancers [42]. Given these, the genomic regions that we identified as enhancer candidates are possibly involved in tissue-specific expression and functions of *Trps1*. Skeletal phenotypes of our enhancer deleted mice further support this notion.

Individual deletions of Enh1, Enh2, and Enh3 caused subtle phenotypes in mice, suggesting that each of the single enhancer is functionally dispensable for normal skeletal development or they have functional redundancy. Importantly, these mutants

For Peer Review

displayed a mildly deformed acetabulum when the *Trps1* gene dosage was further reduced by deletion of one allele of *Trps1*. This result raises the possibility that each enhancer contributes to hip joint maturation when the genetic robustness of *Trps1* expression is reduced. This idea was supported by the observation that more severe acetabular defects were present when Enh2 and Enh3 were simultaneously deleted. The coincidence of the defective anatomical site observed in different *Trps1* enhancer mutant strains and the difference in the severities observed strongly indicate that normal acetabular morphogenesis depends upon a sufficient *Trps1* gene dose.

Trps1$^{\Delta int/-}$ mice display the most severe growth defects among the mice we tested; however, these defects became apparent postnatally. Recent evidence suggests that postnatal skeletal growth is driven by the activation of the stem cell niche that appears in synchronization with the maturation of SOC [43; 44]. The postnatal growth defects and defective SOC formation in *Trps1*$^{\Delta int/-}$ mice suggest that the diminished chondrocyte stem cell population may be the cause of their gradual pronounced shortening of body length.

2. Skeletal pathologies in TRPS patients and TRPS mouse models

Greater than 50% of patients with TRPS exhibit developmental dysplasia of the hip [2; 13]. These malformations include coxa plana (resembling the femoral head morphology

For Peer Review

in Perthes disease), coxa magna (relative enlargement of the femoral head), and coxa vara (reduction of the femoral neck shaft angle). Possibly due to these abnormal developments, older patients with TRPS display hip abnormalities associated with degenerative coxarthrosis. Although these reports suggest important roles for Trps1 in hip joint development, they have not been investigated by mouse genetics to date. The present study addressed this issue. Conventional *Trps1*$^{-/-}$ mice exhibited a reduction in the size of the ilium, ischium, and pubis. The width of the pelvic floor was narrower, and the subpubic angle was more acute in *Trps1*$^{-/-}$ embryos. As the pubic symphysis is normally observed in *Trps1*$^{-/-}$ mice, the short anterior-posterior length of the pelvis appears to be compensated for by the bending of the pelvis at the ilium and ischium/pubis border (Suppl. Fig. 5).

As the pelvis and femur phenotypes of *Trps1*$^{\Delta int/\Delta int}$ mice were similar to those of *Trps1*$^{-/-}$ mice at the perinatal stage, we examined the hip joint morphology of *Trps1*$^{\Delta int/\Delta int}$ mice at the adult stage. The pubic bone element was particularly affected in *Trps1*$^{\Delta int/\Delta int}$ mice, and consequently the acetabulum of the pubic bone region was poorly formed, ultimately resulting in undercoverage of the femoral heads. These morphological changes often lead to altered joint load and motion, thus causing the onset of degenerative joint pathologies [45; 46]. These conclusions are further supported by reports correlating an increased risk

For Peer Review

of osteoarthritis with morphological deformities of the proximal femur and acetabulum [47; 48].

Trps1$^{\Delta int/-}$ mice displayed patella formation in the normal position; however, in adult mice that survived to the mature stage, medial patellar dislocation was observed in all examined knees. Significantly, it has been reported that some patients with TRPS display an abnormal patella with recurrent dislocation [49]. The patella is the largest sesamoid bone embedded in the quadriceps tendon and facilitates musculoskeletal function. Development of the patella was originally thought to occur inside the tendons in response to mechanical signals from the attaching muscles [50]; however, it is now established that in the mouse embryo, the patella initially develops as a bony process at the anterodistal surface of the femur from Sox9 and Scleraxis double-positive progenitor cells and separates from the distal femur via Gdf5-positive joint formation [51]. Postnatally, the patella plays a crucial role in knee mechanics and stability and facilitates hind limb function and locomotion [52]. The patella increases the distance between the quadriceps and knee, and thereby increasing the moment arm of the muscle and enhancing its extension force by 50% [53]. The normal patellar position in newborn *Trps1*$^{\Delta int/-}$ pups indicates that patella development initiates normally at the correct location, and the dislocation occurred postnatally in the mutants. The patella stability

For Peer Review

involves a balance between the stabilizing patellofemoral ligaments, the osteoarticular surface, the position of the patella (high riding patella; patella alta), decreased depth or flattened trochlear groove, and the muscular actions of the quadriceps muscles [54]. 3D-CT images of the distal femur of the *Trps1*$^{\Delta int/-}$ mice indicate the flattened surface at the femoral trochlear groove at 3- and 6-months-of-age. The medial and lateral facets of the groove are not obvious but rather exhibit convexity, ultimately resulting in apparent trochlear dysplasia [55]. Interestingly, the medial fabella, a sesamoid bone embedded in the medial head of the gastrocnemius muscle, exhibited a severe reduction in size. It is important to note that in quadrupedal mammals, the fabella is believed to play a role very similar to that of the patella in redirecting the extension forces of the knee joint from one point to another [56]. The exact causes of the flattened femoral trochlear groove and reduced medial fabella size are not clear. Skin and joint laxity is a characteristic feature of patients with TRPS. These features of TRPS have been described as symptoms that are similar to those observed in patients with Ehlers-Danlos syndrome. Importantly, a mouse model of Ehlers-Danlos syndrome exhibited severe growth retardation, delays in SOC formation, and patellar dislocation, all of which were observed in *Trps1*$^{\Delta int/-}$ mice [57].

For Peer Review

3. The *Trps1*$^{\Delta int/\Delta int}$ mouse strain as a novel TRPS disease model for postnatal studies.

The etiologies of TRPS have been investigated using several animal models of TRPS. Most of these studies were performed using homozygous knockout mice. Although they are useful, they possess significant limitations due to their early postnatal lethality. Patients with TRPS exhibit various postnatal diseases. These conditions include skeletal dysplasia, coxarthrosis, and progressive short stature [2]. Our novel *Trps1*$^{\Delta int/\Delta int}$ mouse strain could partially overcome this limitation, contributing to the postnatal studies of TRPS pathologies.

For Peer Review

Materials and Methods

1. ATAC-seq and ChIP-seq of mouse costal chondrocytes.

Assays for transposase-accessible chromatin using high-throughput sequencing (ATAC-seq) [58] was performed using costal chondrocytes isolated from neonatal mouse ribs [59]. Approximately 50,000 cells were lysed using lysis buffer (10 mM Tris-HCl, pH 7.4, 10 mM NaCl, 3 mM $MgCl_2$, and 0.1% IGEPAL CA-630) to release the nuclei and then treated with Tn5 transposase (Illumina #FC121-1030) at 37°C for 30 minutes. The adaptors were ligated and amplified using polymerase chain reaction (PCR) for high-throughput sequencing. Paired-end sequencing (100 bp) was performed using an Illumina HiSeq platform at the Osaka University Research Institute for Microbial Diseases NGS Core Facility. Qualified sequencing reads were aligned to the reference genome (mm9) using Bowtie 2 (ver. 2.4.4) [60], and MACS2 was used for peak calling [61]. Two biological replicates were analyzed for ATAC-seq. Chromatin immunoprecipitation followed by sequencing (ChIP-seq) was performed using antibodies against histone modifications [62]. Primary chondrocytes were crosslinked with 1% formaldehyde for 5 min. Crosslinking was quenched with 1 M glycine for 5 min. Cells were lysed and chromatin was sonicated with Covaris M220. Fragmented DNA was immunoprecipitated using an antibody against acetylated H3 lysine 27 (H3K27ac) (Cell Signaling Technology

For Peer Review

(CST) #8173, 2 μg per reaction) or against demethylated H3 lysine 4 (H3K4me2) (CST, #9725, 2 μg per reaction). H3K27ac is associated with active enhancer regions, while H3K4me2 is predominantly enriched around the functional cis-regulatory elements as well as transcription start sites (TSS) [63]. All immunoprecipitation was performed for 4 hours at 4°C. ChIP samples were washed, eluted at 65°C for 30min, and reverse crosslinked at 65°C overnight. DNA was purified using DNA purification spin columns. Library preparation, sequencing, and peak calling were performed as described above. ATAC-seq and ChIP-seq data have been deposited in the NCBI Gene Expression Omnibus with the accession code GSE237889 (https://www.ncbi.nlm.nih.gov/geo/query/acc.cgi?acc=GSE237889).

2. Luciferase assays

The enhancer 2 (Enh2; 2,981 bp) and enhancer 3 (Enh3; 5,370 bp) genomic fragments were amplified using a high-fidelity KODFX DNA polymerase (TOYOBO, Osaka, Japan) by the primer sequences listed in Table 1. The A-tailed fragments were subcloned into the pTA2 vector (TOYOBO). The inserts were released and subcloned into the pGL3-promoter vector (Promega) to generate Enh2-Luciferase and Enh3-Luciferase constructs. The Enh3 fragment was inserted into the Enh2-Luciferase clone to generate an Enh2-Enh3-Luciferase construct. Firefly Luciferase vectors and pTK-Renilla luciferase vector

For Peer Review

(Promega) were transfected into ATDC5 chondrocytic cell line seeded onto 12-well culture plates [64; 65] with ScreenFect A (Fujifilm, Osaka, Japan) for 6 h. The cells were rinsed once with phosphate buffered saline (PBS) and then cultured in DMEM/F-12 media (Sigma) supplemented with 10% fetal bovine serum (FBS). After cultured for an additional 40 h, the cells were lysed with 200 µl of luciferase lysis buffer (Promega). Luciferase measurements and normalization were performed as described previously [66; 67]. The experiments were performed in triplicate and performed at least three times, and representative data are presented in the figures.

3. Animals

Conventional *Trps1* knockout mouse strain (*Trps1*$^{-/-}$ mice) has been described previously [5; 8]. *Trps1* enhancer-deleted strains were generated by CRISPR/Cas9 genome editing. ΔEnh1 strain was generated by the deletion of the enhancer 1 (Enh1) sequence, which is located upstream of *Trps1* TSS [31]. Enh2 and Enh3 are located in the first intron of the *Trps1* gene; approximately 3 kb (Enh2), 4 kb (Enh3), and 20 kb genomic regions containing both of the enhancers were deleted in ΔEnh2, ΔEnh3, and Δint strains, respectively. The guide RNA sequences used for genome editing are listed in Table 1. crRNA, tracrRNA, and the Cas9 protein complex were electroporated into fertilized eggs (C57BL/6J) and cultured *in vitro* until the two-cell stage. Eggs were implanted into the

For Peer Review

fallopian tubes of pseudo-pregnant female mice. F0 mice with successful deletions were initially mated with C57BL/6J wild-type (WT) mice (Japan SLC, Inc., Shizuoka, Japan) for germline transmission. Non-mosaic heterozygotes of F1 males and females were used for breeding. To generate *Trps1* double heterozygotes including *Trps1*$^{\Delta int/-}$ mice, we crossed *Trps1* enhancer-deleted strain with conventional *Trps1* heterozygous knockout strain. Genotyping was performed using the genomic DNA purified from tail clips or skin tissue. Primer used for genotyping are listed in Table 2.

Body weight was measured every week after weaning until week 9. For embryonic stage sample preparation, noon of the day the vaginal plug appeared was considered as embryonic day (E) 0.5. Pregnant female mice were humanely euthanized, and embryos were collected by C-section. All animal experiments were approved by the Animal Experiment Committee of the Osaka University Graduate School of Dentistry (Animal Protocol #29-016-0). Experimental procedures were performed according to the Association for Assessment and Accreditation of Laboratory Animal Care International and local guidelines. The rooms were maintained at 22 to 26 degrees under 12 h light/dark cycle.

4. Skeletal analysis

Alizarin red and alcian blue staining of bone and cartilage was performed as previously

For Peer Review

described [68]. Three-dimensional micro-computed tomography (3D-CT) images of the pelvic region were captured by R-mCT2 (Rigaku, Tokyo, Japan) at Field of view (FOV) 20 at 90V and 160μA. Images were created using three-dimensional reconstruction imaging software (TRI/ 3D-BON; RATOC System Engineering Co., Ltd., Tokyo, Japan). The psoas valley depth was measured according to a previous report [69]. Briefly, a straight line passing through the upper and lower hip labra was drawn. A line perpendicular to and crossing the center of the femoral head was drawn. The lengths of the psoas valleys depth were measured using the ImageJ software. As there could be sex-specific variations in pelvic girdle morphology, we used only male mice for the postnatal study. Sex was not determined for the embryonic stage samples used in this study.

4. Total RNA isolation from primary costal chondrocytes and reverse transcription-quantitative PCR (RT-qPCR).

Postnatal day 3 (PNd3) pups were humanely euthanized by injecting them with an overdose of anesthetic drugs, and various tissues or organs were dissected in cold PBS under a stereoscopic microscope. Each tissue and organ was stored separately in 350 μl buffer RLT (Qiagen, Hilden, Germany) supplemented with beta-mercaptoethanol. Total RNA was prepared using an RNeasy Plus kit (Qiagen) according to the manufacturer's

For Peer Review

instructions. Samples obtained from both WT and *Trps1*$^{\Delta int/\Delta int}$ animals were homogenized and subjected to the column purification processes. WT, *Trps1*$^{\Delta Enh2/\Delta Enh2}$, *Trps1*$^{\Delta Enh3/\Delta Enh3}$, and *Trps1*$^{\Delta int/\Delta int}$ were used for preparation of the neonatal costal chondrocytes. Cells were harvested as described previously [59]. The cells were cultured in DMEM supplemented with 10% FBS and antibiotics. Cells from passage two were used for qPCR analysis. Purified total RNA (1 μg) was reverse-transcribed into cDNA using ReverTra Ace (TOYOBO). THUNDERBIRD SYBR qPCR mix (TOYOBO) was used for real-time PCR on a 20 μl reaction scale. A MiniOpticon qPCR apparatus equipped with CFX managing software (Bio-Rad Laboratories, Berkeley, CA, USA) was used for reaction and data acquisition as described previously [70]. The primers used for real-time PCR were 5'-CAG CTC CCA AGA GCA GAC AAA-3' and 5'-GTC AGG CAA TTG GCA CAA AAA-3' for *Trps1*, and the primer sequence for *Hprt1* has been described previously [71].

3. *In situ* hybridization and immunohistochemistry

Sectional *in situ* hybridization was performed as previously described [5]. Transverse cryo-sections of E12.5 embryos were prepared at thickness of 14 microns. Sense and antisense *Trps1* cRNA probes were synthesized using the NM_032000.2 nt.412-1291 sequence as a template. Immunohistochemistry was performed on transverse cryo-

For Peer Review

sections of E12.5 wildtype and *Trps1*$^{-/-}$ embryos using anti-Sox9 rabbit monoclonal antibody (1:400 #D8G8H, CST, Danvers MA). Endogenous peroxidase activity was inhibited by 0.3% H_2O_2 for 15 min at RT. Biotinylated anti-rabbit IgG (4 μg/ml Vector Laboratories, Burlingame, CA) and HRP-conjugated streptavidin (2 μg/ml; Abcam, Cambridge, UK) were used for the following reactions. Color development was performed using 3,3'-Diaminobenzidine with nickel enhancement. Normal rabbit IgG (CST) was used instead of the primary antibody as a negative control. The stained sections were then dehydrated and covered with coverslips. Postnatal animals were fixed by perfusion under deep anesthesia. The hindlimbs were further fixed in 4% paraformaldehyde for more than 16 hours at 4 degrees. Then, the samples were decalcified in 10% ethylenediamine tetraacetic acid (EDTA) for 10 to 14 days at 4 degrees Celsius. The decalcified samples were dehydrated, embedded in paraffin, and then sectioned at a 4-micron thickness. Stained images were captured using an Axioskop 2 plus equipped with an Axiocam 208 (Carl Zeiss Microscopy, Jena, Germany) or BZ-X800 with appropriate software (Keyence).

4. Statistical analysis.

The results are expressed as the means ± standard deviation (SD). The mean values of two samples were compared using Student's *t-test*. Statistical significance was set at *P*

For Peer Review

< 0.05. Multiple comparison of more than three samples were analyzed by one-way analysis of variance (ANOVA), followed by Tukey's post-hoc test using GraphPad Prism8 software. At least three animals per each genotype were used for all the analysis.

For Peer Review

Acknowledgements

This work was supported by Grants-in-Aid for Scientific Research from MEXT to MA (17K11611, 22K06295), JSPS KAKENHI JP16H06276 (AdAMS) to MA, and the Takeda Science Foundation for SI. The authors acknowledge Dr. Yasuteru Muragaki for sharing the *Trps1* knockout strain; Dr. Ryouji Yao, Dr. Hiroshi Takano, Dr. Hitomi Yamanaka, and Dr. Masahito Ikawa for their help with mouse generation; and Ms. Mariko Kasai for the technical assistance.

Declaration of interests

None.

Author contributions

N.S., S.O., M.A. conceived of the study, T.I., S.A., S.O., M.A. supervised the work, N.S., K.H., S.I., S.O., M.A. designed the experiments, N.S., C.I-Y., Y.I., R.K., K.H., S.O., M.A. performed the experiments and analyzed results, N.S., S.O., M.A. wrote the manuscript with input from all authors.

For Peer Review

References

1. Momeni, P., Glockner, G., Schmidt, O. et al. Mutations in a new gene, encoding a zinc-finger protein, cause tricho-rhino-phalangeal syndrome type I. *Nat Genet* 2000;**24**:71-74.

2. Ludecke, H.J., Schaper, J., Meinecke, P. et al. Genotypic and phenotypic spectrum in tricho-rhino-phalangeal syndrome types I and III. *Am J Hum Genet* 2001;**68**:81-91.

3. Le Saout, J., Lefevre, C., Kerboul, B. et al. Osteochondritis of the hip and the tricho-rhino-phalangeal syndrome. *Ann de Chirurgie* 1984;**38**:357-362.

4. Itoh, S., Kanno, S., Gai, Z., et al. Trps1 plays a pivotal role downstream of Gdf5 signaling in promoting chondrogenesis and apoptosis of ATDC5 cells. *Genes Cells* 2008;**13**:355-363.

5. Michikami, I., Fukushi, T., Honma, S. et al. Trps1 is necessary for normal temporomandibular joint development. *Cell Tis Res* 2012;**348**:131-140.

6. Napierala, D., Sam, K., Morello, R.et al. Uncoupling of chondrocyte differentiation and perichondrial mineralization underlies the skeletal dysplasia in tricho-rhino-phalangeal syndrome. *Hum Mol Genet* 2008;**17**:2244-2254.

7. Napierala, D., Sun, Y., Maciejewska, I.et al. Transcriptional repression of the Dspp gene leads to dentinogenesis imperfecta phenotype in Col1a1-Trps1 transgenic mice. *J Bone Min Res* 2012;**27**:1735-1745.

For Peer Review

8. Suemoto, H., Muragaki, Y., Nishioka, K. et al. Trps1 regulates proliferation and apoptosis of chondrocytes through Stat3 signaling. *Dev Biol* 2007;**312**:572-581.

9. Kanno, S., Gui, T., Itoh, S.et al. Aberrant expression of the P2 promoter-specific transcript Runx1 in epiphyseal cartilage of Trps1-null mice. *Exp Mol Pathol* 2011;**90**:143-148.

10. Nishioka, K., Itoh, S., Suemoto, H. et al. Trps1 deficiency enlarges the proliferative zone of growth plate cartilage by upregulation of Pthrp. *Bone* 2008;**43**:64-71.

11. Wuelling, M., Kaiser, F.J., Buelens, L.A. et al. Trps1, a regulator of chondrocyte proliferation and differentiation, interacts with the activator form of Gli3. *Dev Biol* 2009;**328**:40-53.

12. Wuelling, M., Schneider, S., Schrother, V.A. et al. Wnt5a is a transcriptional target of Gli3 and Trps1 at the onset of chondrocyte hypertrophy. *Dev Biol* 2020;**457**:104-118.

13. Maas, S.M., Shaw, A.C., Bikker, H. et al. Phenotype and genotype in 103 patients with tricho-rhino-phalangeal syndrome. *Eur J Med Genet* 2015;**58**:279-292.

14. Fontaine, G., Maroteaux, P., Farriaux, J.P. et al. The tricho-rhino-phalangeal syndrome. *Arch Fr Pediatr* 1970;**27**:635-647.

15. Beals, R.K. Tricho-rhino-phalangeal dysplasia. Report of a kindred. *J Bone Joint Surg Am* 1973;**55**:821-826.

For Peer Review

16. Felman, A.H., Frias, J.L. The trichorhinophalangeal syndrome: study of 16 patients in one family. *AJR Am J Roent* 1977;**129**:631-638.

17. Peltola, J., Kuokkanen, K. Tricho-rhino-phalangeal syndrome in five successive generations: Report on a family in Finland. *Acta Dermato-Vener* 1978;**58**:65-68.

18. Howell, C.J., Wynne-Davies, R. The tricho-rhino-phalangeal syndrome. A report of 14 cases in 7 kindreds. *J Bone Joint Surg Br* 1986;**68**:311-314.

19. Don, E.K., Currie, P.D., Cole, N.J. The evolutionary history of the development of the pelvic fin/hindlimb. *J Anat* 2013;**222**:114-133.

20. Yano, T., and Tamura, K. The making of differences between fins and limbs. *J Anat* 2013;**222**:100-113.

21. Malashichev, Y., Borkhvardt, V., Christ, B. et al. Differential regulation of avian pelvic girdle development by the limb field ectoderm. *Anat Embryol* 2005;**210**:187-197.

22. Delaere, O., Kok, V., Nyssen-Behets, C. et al. Ossification of the human fetal ilium. *Acta Anat* 1992;**143**:330-334.

23. Ponseti, I.V. Growth and development of the acetabulum in the normal child. Anatomical, histological, and roentgenographic studies. *J Bone Joint Surg Am* 1978;**60**:575-585.

24. Harrison, T.J. The influence of the femoral head on pelvic growth and acetabular

For Peer Review

652 form in the rat. *J Anat* 1961;**95**:12-24.

653 25. Harris-Hayes, M., Royer, N.K. Relationship of acetabular dysplasia and
654 femoroacetabular impingement to hip osteoarthritis: a focused review. PM & R : *J Inj*
655 *Funct Rehab* 2011;**3**:1055-1067 e1051.

656 26. Anderson, F.A., Jr., Huang, W., Friedman, R.J. et al. Prevention of venous
657 thromboembolism after hip or knee arthroplasty: findings from a 2008 survey of US
658 orthopedic surgeons. *J Arthro* 2012;**27**:659-666 e655.

659 27. Diesel, C.V., Ribeiro, T.A., Scheidt, R.B. et al. The prevalence of femoroacetabular
660 impingement in radiographs of asymptomatic subjects: a cross-sectional study. *J Clin*
661 *Exp Res Hip Pathol Ther* 2015;**25**:258-263.

662 28. Storer, S.K., Skaggs, D.L. Developmental dysplasia of the hip. *Am Fam Phys*
663 2006;**74**:1310-1316.

664 29. McWilliams, D.F., Doherty, S.A., Jenkins, W.D. et al. Mild acetabular dysplasia and
665 risk of osteoarthritis of the hip: a case-control study. *Annals Rheum Dis* 2010;**69**:1774-
666 1778.

667 30. Jacobsen, S., Sonne-Holm, S. Hip dysplasia: a significant risk factor for the
668 development of hip osteoarthritis. A cross-sectional survey. *Rheumatology* 2005;**44**:211-
669 218.

For Peer Review

31. Nomir, A.G., Takeuchi, Y., Fujikawa, J. et al. Fate mapping of Trps1 daughter cells during cardiac development using novel Trps1-Cre mice. *Genesis* 2016;**54**:379-388.

32. Xie, M., Gol'din, P., Herdina, A.N. et al. Secondary ossification center induces and protects growth plate structure. *eLife* 2020;9.

33. Kopydlowski, N.J., Tannenbaum, E.P., Smith, M.V. et al. Characterization of Human Anterosuperior Acetabular Depression in Correlation With Labral Tears. *Orthop J Sports Med* 2014;**2**:2325967114551328.

34. Chatterjee, S., Ahituv, N. Gene Regulatory Elements, Major Drivers of Human Disease. *Annu Rev Genomics Hum Genet* 2017;**18**:45-63.

35. Dwyer, K., Agarwal, N., Pile, L. et al. Gene Architecture Facilitates Intron-Mediated Enhancement of Transcription. *Front Mol Biosci* 2021;**8**:669004.

36. Nilsen, T.W., Graveley, B.R. Expansion of the eukaryotic proteome by alternative splicing. *Nature* 2010;**463**:457-463.

37. Niehrs, C., Luke, B. Regulatory R-loops as facilitators of gene expression and genome stability. Nature reviews *Mol Cell Biol* 2020;**21**:167-178.

38. Ding, F., Elowitz, M.B. Constitutive splicing and economies of scale in gene expression. *Nat Struct Mol Biol* 2019;**26**:424-432.

39. Laxa, M. Intron-Mediated Enhancement: A Tool for Heterologous Gene Expression

For Peer Review

688 in Plants? *Front Plant Sci* 2016;**7**:1977.

689 40. Shaul, O. How introns enhance gene expression. *Int J Biochem Cell Biol* 2017;**91**:145-

690 155.

691 41. Ott, C.J., Blackledge, N.P., Kerschner, J.L. et al. Intronic enhancers coordinate

692 epithelial-specific looping of the active CFTR locus. *Proc Nat Acad Sci* 2009;**106**:19934-

693 19939.

694 42. Borsari, B., Villegas-Miron, P., Perez-Lluch, S., et al. Enhancers with tissue-specific

695 activity are enriched in intronic regions. *Genome Res* 2021;**31**:1325-1336.

696 43. Mizuhashi, K., Nagata, M., Matsushita, Y. et al. Growth Plate Borderline

697 Chondrocytes Behave as Transient Mesenchymal Precursor Cells. *J Bone Min Res*

698 2019;**34**:1387-1392.

699 44. Newton, P.T., Li, L., Zhou, B. et al. A radical switch in clonality reveals a stem cell

700 niche in the epiphyseal growth plate. *Nature* 2019;**567**:234-238.

701 45. Jacobsen, S., Sonne-Holm, S., Lund, B.et al. Pelvic orientation and assessment of hip

702 dysplasia in adults. *Acta Orthop Scand* 2004;**75**:721-729.

703 46. Jacobsen, S., Sonne-Holm, S., Soballe, K. et al. Radiographic case definitions and

704 prevalence of osteoarthrosis of the hip: a survey of 4 151 subjects in the Osteoarthritis

705 Substudy of the Copenhagen City Heart Study. *Acta Orthop Scand* 2004;**75**:713-720.

For Peer Review

47. Beck, M., Kalhor, M., Leunig, M. et al. Hip morphology influences the pattern of damage to the acetabular cartilage: femoroacetabular impingement as a cause of early osteoarthritis of the hip. *J Bone Joint Surg Br* 2005;**87**:1012-1018.

48. Ahedi, H.G., Aspden, R.M., Blizzard, L.C. et al. Hip Shape as a Predictor of Osteoarthritis Progression in a Prospective Population Cohort. *Arth Care Res* 2017;**69**:1566-1573.

49. Puliyel, J.M., Puliyel, M.M., Varughese, S. The trichorhinophalangeal syndrome with repeated dislocation of the patella. *Clin Genet* 1992;**41**:139-142.

50. Sarin, V.K., Erickson, G.M., Giori, N.J. et al. Coincident development of sesamoid bones and clues to their evolution. *Anat Rec* 1999;**257**:174-180.

51. Eyal, S., Blitz, E., Shwartz, Y. et al. On the development of the patella. *Development* 2015;**142**:1831-1839.

52. Sutton, F.S., Jr., Thompson, C.H., Lipke, J. et al. The effect of patellectomy on knee function. *J Bone Joint Surg Am* volume 1976;**58**:537-540.

53. Schindler, O.S., Scott, W.N. Basic kinematics and biomechanics of the patello-femoral joint. Part 1: The native patella. *Acta Orthop Bel* 2011;**77**:421-431.

54. Bicos, J., Carofino, B., Andersen, M. et al. Patellofemoral forces after medial patellofemoral ligament reconstruction: a biomechanical analysis. *J Knee Surg*

For Peer Review

2006;**19**:317-326.

55. McConnell, J. Rehabilitation and nonoperative treatment of patellar instability. *Sp Med Arthrosc Rev* 2007;**15**:95-104.

56. Driessen, A., Balke, M., Offerhaus, C. et al. The fabella syndrome - a rare cause of posterolateral knee pain: a review of the literature and two case reports. *BMC Muscul Dis* 2014;**15**:100.

57. Zhu, M., Metzen, F., Hopkinson, M. et al. Ablation of collagen XII disturbs joint extracellular matrix organization and causes patellar subluxation. *iScience* 2023;26:107225.

58. Buenrostro, J.D., Wu, B., Chang, H.Y. et al. ATAC-seq: A Method for Assaying Chromatin Accessibility Genome-Wide. *Cur Prot Mol Biol* 2015;**109**:21 29 21-21 29 29.

59. Gosset, M., Berenbaum, F., Thirion, S. et al. Primary culture and phenotyping of murine chondrocytes. *Nat Protoc* 2008;**3**:1253-1260.

60. Langmead, B., Salzberg, S.L. Fast gapped-read alignment with Bowtie 2. *Nat Methods* 2012;**9**:357-359.

61. Zhang, Y., Liu, T., Meyer, C.A. et al. Model-based analysis of ChIP-Seq (MACS). *Genome Biol* 2008;**9**:R137.

62. Ernst, J., Kheradpour, P., Mikkelsen, T.S. et al. Mapping and analysis of chromatin

For Peer Review

state dynamics in nine human cell types. *Nature* 2011;**473**:43-49.

63. Nakato, R., Sakata, T. Methods for ChIP-seq analysis: A practical workflow and advanced applications. *Methods* 2021;**187**:44-53.

64. Atsumi, T., Miwa, Y., Kimata, K. et al. A chondrogenic cell line derived from a differentiating culture of AT805 teratocarcinoma cells. *Cell Differ Dev* 1990;**30**:109-116.

65. Shukunami, C., Shigeno, C., Atsumi, T. et al. Chondrogenic differentiation of clonal mouse embryonic cell line ATDC5 in vitro: differentiation-dependent gene expression of parathyroid hormone (PTH)/PTH-related peptide receptor. *J Cell Biol* 1996;**133**:457-468.

66. Abe, M., Michikami, I., Fukushi, T. et al. (2010). Hand2 regulates chondrogenesis in vitro and in vivo. *Bone* 2010;**46**:1359-1368.

67. Michikami, I., Fukushi, T., Tanaka, M. et al. Kruppel-like factor 4 regulates membranous and endochondral ossification. *Exp Cell Res* 2012;**318**:311-325.

68. McLeod, M.J. Differential staining of cartilage and bone in whole mouse fetuses by alcian blue and alizarin red S. *Teratology* 1980;**22**:299-301.

69. Kuroda, Y., Rai, A., Saito, M. et al. Anatomical variation of the Psoas Valley: a scoping review. *BMC Muscul Dis* 2020;**21**:219.

70. Takeuchi, Y., Tatsuta, S., Kito, A. et al. Kruppel-like factor 4 upregulates matrix metalloproteinase 13 expression in chondrocytes via mRNA stabilization. *Cell Tissue*

For Peer Review

Res 2020;**382**:307-319.

71. Fujikawa, J., Takeuchi, Y., Kanazawa, S. et al. Kruppel-like factor 4 regulates matrix metalloproteinase and aggrecanase gene expression in chondrocytes. *Cell Tissue Res* 2017;**370**:441-449.

For Peer Review

Legends to Figures

Figure 1. Identification of putative enhancers around the *Trps1* gene.

(A) Open chromatin regions and histone modification (H3K4me2 and H3K27ac) identified by ATAC-seq and ChIP-seq in murine primary costal chondrocytes. Overhead view of the murine *Trps1* genomic region (upper image) and magnified view of the first intron (lower image). The first intron of the murine *Trps1* genomic region is highlighted by a red dotted square. Overlapping regions of ATAC-seq and ChIP-seq peaks within the first intron of *Trps1* are highlighted by a pink box. Enhancer 2 (Enh2; Chr15:50885838-50889066) and enhancer 3 (Enh3; Chr15:50868499-50872947) are labeled with red and blue bars, respectively.

(B) Genomic alignment of the *Trps1* gene loci of multiple species. Evolutionary conserved sequence alignment of multiple genomes was performed using the ECR program from Dcode.org (http://www.dcode.org).

(C) Luciferase reporter assays for Emh2 and Enh3 in chondrocytic ATDC5 cells. Enh2-, Enh3-, or Enh2-Enh3-containing pGL3-promoter luciferase vectors were transfected into chondrocytic ATDC5 cells. Cell lysate was harvested after 40 hours post-transfection for dual-luciferase assay (*$P < 0.05$).

For Peer Review

(D) Luciferase reporter assays for Enh2 deletion mutants in chondrocytic ATDC5 cells. pGL3-promoter luciferase vectors carrying deleted versions of Enh2 were transfected into ATDC5 cells. Cell lysate was harvested after 40 hours post-transfection for dual-luciferase assay (*P < 0.05).

Figure 2. *Trps1*$^{-/-}$ mice display abnormal coxal bone morphogenesis.

(A1) Expression of *Trps1* detected by *in situ* hybridization in the developing hip joint of E12.5 WT embryo. V and D indicate the ventral and dorsal sides, respectively.

(A2 and A3) Sox9 protein localization was detected by immunohistochemistry in the developing hip region of E12.5 WT (A2) and *Trps1*$^{-/-}$ (A3) embryos.

(B and C) Lateral views of the hindlimb (B) and coxal bone (C) of E15.5 WT and *Trps1*$^{-/-}$ embryos. Arrowheads in (C) indicates the mineralized region at the primary ossification center within the ilium.

(D-F) Medial views of hindlimbs (D), coxal bone (E), and pelvic bone (F) of E17.5 WT (left), *Trps1*$^{+/-}$ (mid), and *Trps1*$^{-/-}$ (right) embryos. Double arrows in (E) indicated the rostral-caudal length which is shorter in *Trps1*$^{-/-}$ embryos compared to others. Arrowheads in (E) indicate the reduced range of the mineralized region within the primary ossification center of the ischium and pubis in *Trps1*$^{-/-}$ embryos. In (F), the angle between the ilium and pubis was highlighted. (G)

For Peer Review

The measurements of the ilio-pubic angle show that the angle is smaller in *Trps1*$^{-/-}$ embryos than others (n=3 used for each genotype).

Key; ac: primordium of acetabulum, co: primordium of os coxa, fe: femur, fi: fibula. hg: hindgut. il: ilium, is: ischium, pu: pubis, ti: tibia.

Figure 3. Delayed maturation of the ilio-pubic junction and abnormal psoas valley invagination in *Trps1*$^{\Delta int/\Delta int}$ mice.

(A-D) Ventral view of 3D-CT (A and B) and toluidine blue-stained frontal section (C and D) of the hip joint in the 1-month-old control and *Trps1*$^{\Delta int/\Delta int}$ mice. Arrowheads in (B) indicate the mildly expanded width between the mineralized ilium and pubis in *Trps1*$^{Dint/Dint}$ mice. Double arrows in (C) and (D) indicate the cartilaginous region at the ilio-pubic junction.

(E-H) HE-stained frontal sections (E and F) and ventral views of reconstructed 3D-CT (G and H) of the hip joint in the 3-month-old control and *Trps1* $^{\Delta int/\Delta int}$ mice. The arrowhead in (H) points to the deeply invaginated psoas valley in *Trps1*$^{Dint/Dint}$ mice.

(I and J) Measurement of the psoas valley depth. The measured length is indicated by the double arrow in (I). The data of the 2- to 3-month-old control (n=10) and *Trps1* $^{\Delta int/\Delta int}$ (n=12) mice are shown in (J).

For Peer Review

(K and L) Toluidine blue-stained sections of distal femur of postnatal 10-day-old control (K) and *Trps1* $^{\Delta int/\Delta int}$ (L) mice. The invaginating vascular canals into the initial developing site of the secondary ossification center (SOC) are indicated by arrows. Arrowheads in (K) indicate red blood cells (RBCs) at the central region of the distal epiphysis, while RBCs are rarely observed in the similar femoral domain of *Trps1* $^{\Delta int/\Delta int}$ pups.

(M-T) The distal femoral SOC in the 1-month-old control (M-P) or *Trps1* $^{\Delta int/\Delta int}$ (Q-T) mice. Sections stained with toluidine blue (M, M', Q, and Q') or mRNA detected by *in situ* hybridization for *Col1a1* (N and R), *Col2a1* (O and S), and *Col10a1* (P and T) are shown. Red arrowheads in (Q') and (S) indicate the remaining cartilage tissue and chondrocytes left behind at the developing SOC.

Key; fh: femoral head, il: ilium, isc: ischium, pu: pubis.

Figure 4. Skeletal defects in 3-month-old *Trps1*$^{\Delta int/-}$ mice.

(A and B) Ventral views of the dissected anatomy of the hip joint region in the control (A) and *Trps1*$^{\Delta int/-}$ (B) mice. Red dashed lines indicate the acetabular rim, which shows smooth parabolic shape and wedged-shape in the control and *Trps1*$^{\Delta int/-}$ mice, respectively.

For Peer Review

(C and D) Ventral views of reconstructed 3D-CT of hip joint in the control (C) and *Trps1*$^{\Delta int/-}$ (D) mice. Arrowheads highlight deeply invaginated psoas valley, resulting in severe under-coverage of the femoral head within the acetabulum in *Trps1*$^{\Delta int/-}$ mice (D).

(E-H) Transverse sections of the hip joint stained with HE (E and F) and toluidine blue (G and H) in the control (E and G) and *Trps1*$^{\Delta int/-}$ (F and H) mice. (G) and (H) show magnified views of areas surrounded by squares in (E) and (F), respectively, on serial sections. Arrowheads in (H) point to the toluidine blue-positive remaining cartilaginous tissue at the ilio-pubic junction in *Trps1*$^{\Delta int/-}$ mice.

(I-L) Frontal (I and J) and medial (K and L) views of reconstructed 3D-CT of knee joints in the control (I and K) and *Trps1*$^{\Delta int/-}$ (J and L) mice. Medially dislocated patella in *Trps1*$^{\Delta int/-}$ mice is labelled as pt* in (J) and (L). The arrowheads in (J) points to the flattened trochlear groove in *Trps1*$^{Dint/-}$ mice. Arrowheads in (K) and (L) point to the fabella formed within the lateral head of the gastrocnemius muscle. Red dashed lines indicate a round parabolic and straightly shaped surface of the distal femur in the control (K) and *Trps1*$^{\Delta int/-}$ mice (L), respectively. See also (M) and (N).

(M and N) Tomography images at the sagittal mid-planes of the distal femurs in control (M) and *Trps1*$^{\Delta int/-}$ (N) mice. Red dashed lines indicate articular surface of the distal femur in the control (M) and *Trps1*$^{\Delta int/-}$ (N) mice. Epiphyseal bone marrow space is labelled with yellow asterisks.

For Peer Review

(O) Ventral views of the 2-day-old knees in the control (left) and *Trps1*$^{\Delta int/-}$ (right) mice. White arrowheads in point to the stained patella.

(P-S) Low (P and Q) and high (R and S) magnified sagittal images of the distal femurs in the control (P and R) and *Trps1*$^{\Delta int/-}$ (Q and S) mice. Sections were stained with toluidine blue. Double arrows in (R) and (S) indicate epiphyseal growth plate chondrocytes. The asterisk in (S) indicate abnormal accumulation of the toluidine blue-positive cartilage tissue.

Key; co: os coxa, fh: femoral head, fi; fibula, poc: primary ossification center, pt: patella, pt*; dislocated patella, soc: secondary ossification center, ti: tibia.

For Peer Review

Strain	gRNA1	gRNA2
ΔEnh1	TCCACTCCTCCCCGTTGCAAagg	GGTTAATACATGCTGGTCTTtgg
ΔEnh2	CGCTGCTGCAAGTTTTCTGGggg	ACGGGGAGCAGACTAGGCACcgg
ΔEnh3	CAGGCAAGATCAGTTCCCAAggg	ACTTTAGGAACAAAACACCagg
ΔEnh2/3 (Δint)	CGCTGCTGCAAGTTTTCTGGggg	CAGGCAAGATCAGTTCCCAAggg

Table 1. Sequences of guide RNAs used in this study

allele	Forward primer	Reverse primer
Trps1 mut	CCACACACTATTTTCCATGGG	CCCCTTCTATCGCCTTCTTGA
Trps1 wt	TAGTAAAGCAGGCCGTGAAG	ACCCAAAGGTCACTTACTGG
Enh1 mut	TTGCCTGATACTGCAGAGT	TGAGGTTGATATGGTTTTCTG
Enh1 wt	AATCAGTGAAAAATATTTGAG	TGAGGTTGATATGGTTTTCTG
Enh2 mut	GCAAGCTCATACAACTTGCCTGT	ACTCCCCCAATTCCTCTTTTCTC
Enh2 wt	GACGGGTATACCAGGAGAGGATG	ACTCCCCCAATTCCTCTTTTCTC
Enh3 mut	TAGTCAAGTCCACAGGTGGGAAA	AGGACTTCCACTTTACGGAAGC
Enh3 wt	TAGTCAAGTCCACAGGTGGGAAA	ATAGAACAAGTGGCTCCCAGCTC
Enh2/3 mut (Δint mut)	TAGTCAAGTCCACAGGTGGGA AA	ACTCCCCCAATTCCTCTTTTCTC
Enh2/3 wt (Δint wt)	GAAAATGGACCCTGAGGCTTATG	AAAATGCAAGCTTGGTTTGGTTT

Table 2. List of genotyping primers used in this study

For Peer Review

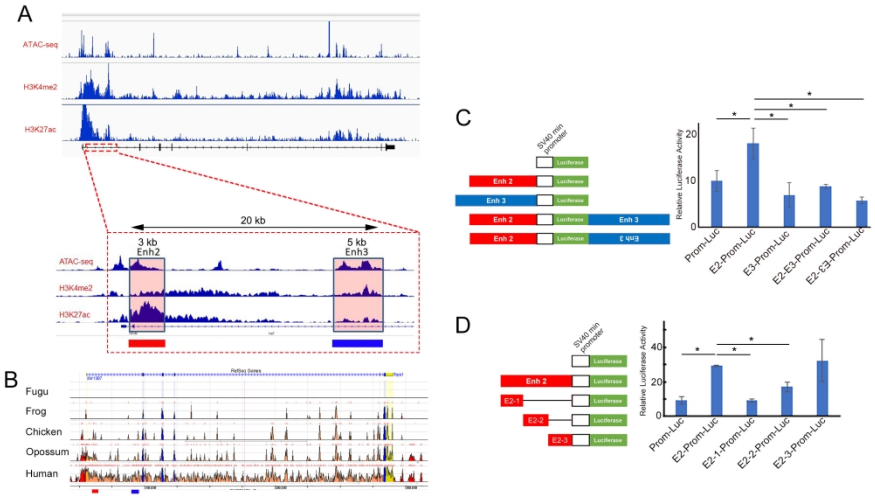

Figure 1

279x215mm (300 x 300 DPI)

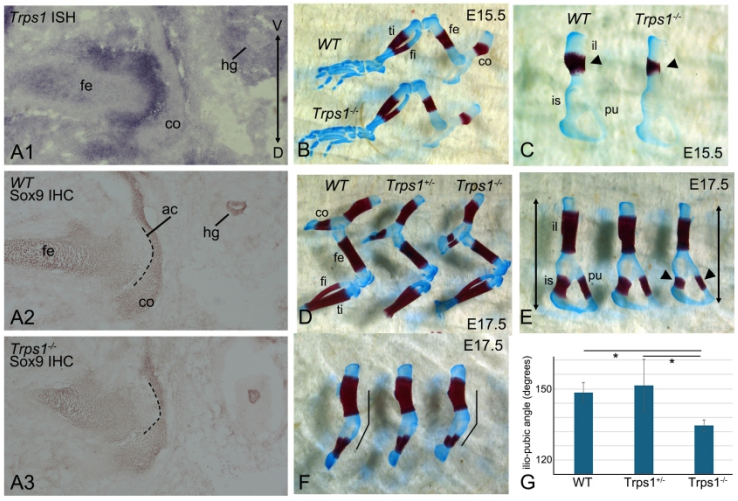

Figure 2

279x215mm (300 x 300 DPI)

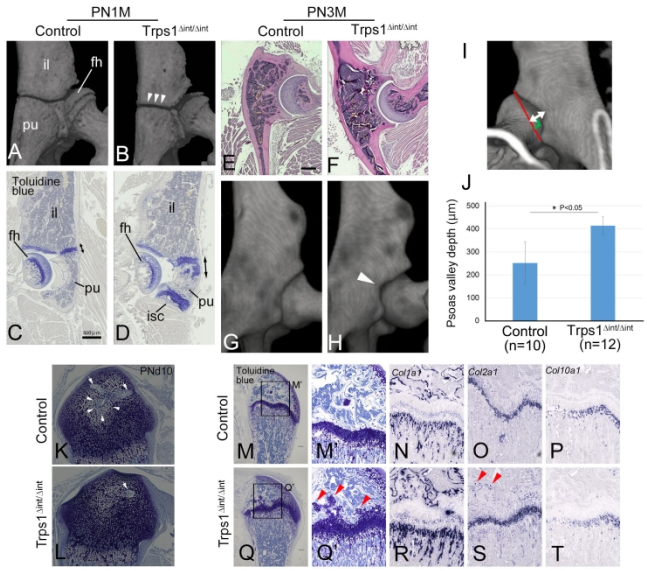

Figure 3

Figure 3

297x209mm (300 x 300 DPI)

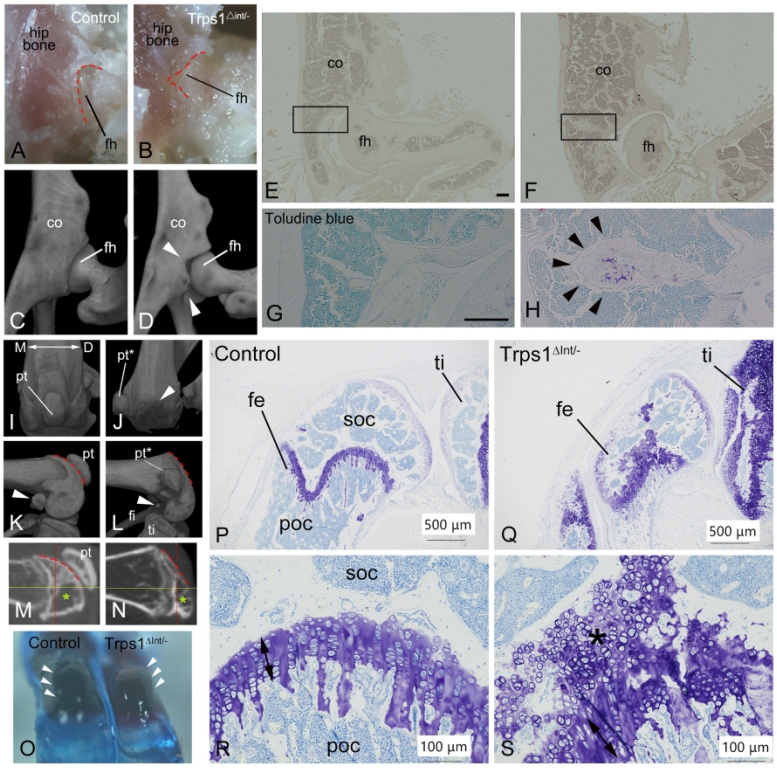

Figure 4

215x279mm (300 x 300 DPI)